TU Delft

MASTER THESIS

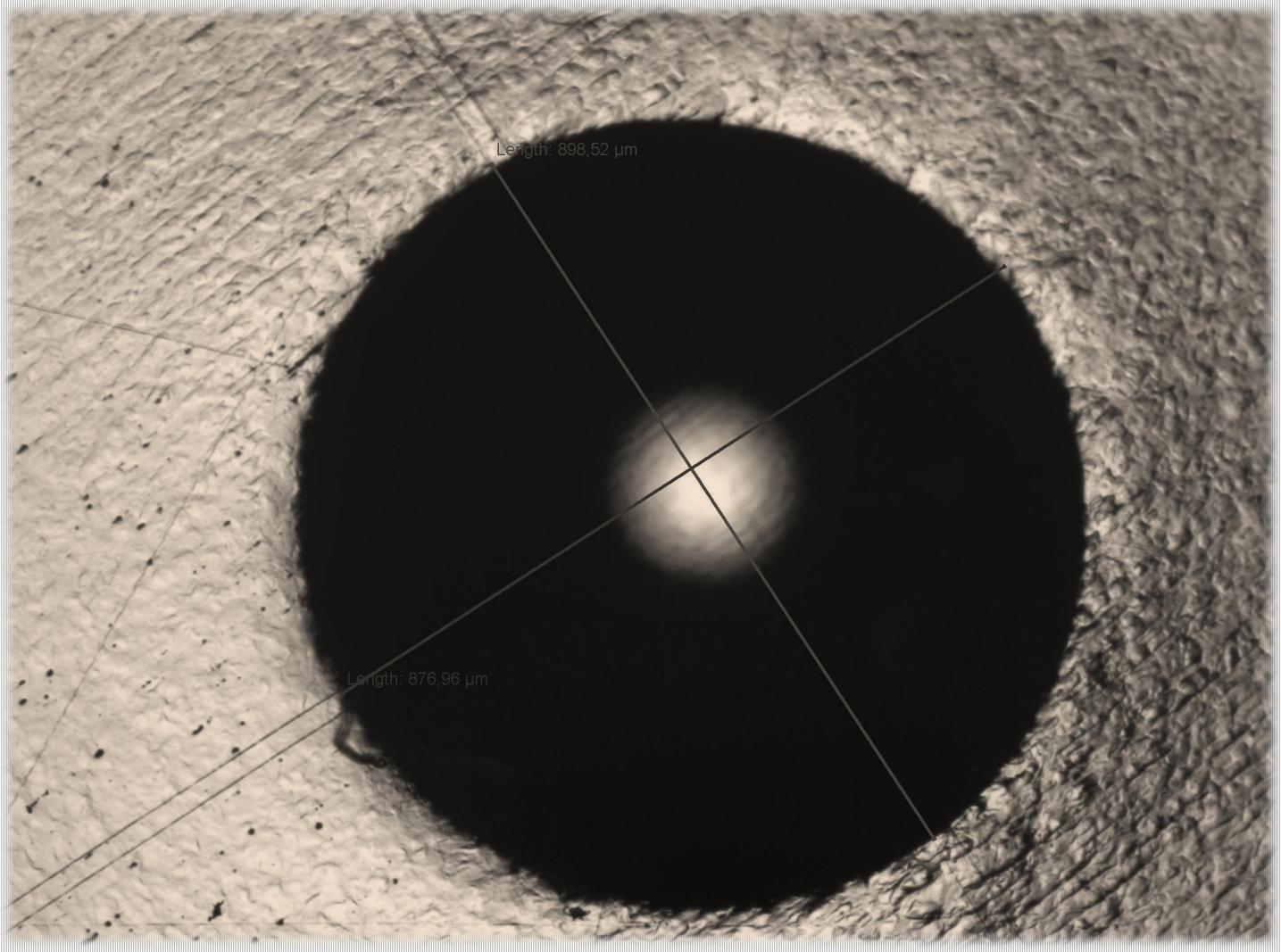

A Novel Micro-Indentation Based Method for Local Mechanical Property Characterization

Qinyi Zheng February of 2024

A Novel Micro-Indentation Based Method for Local Mechanical Property Characterization

THESIS

submitted in partial fulfillment of the
requirements for the degree of

MASTER OF SCIENCE

in

MATERIAL SCIENCE AND ENGINEERING

by

Qinyi Zheng
(Student ID: 5595886)

Supervisor:	Dr. Vera Popovich, Department of MSE, TU Delft
Daily supervisor:	Ir. Niels Troost, Department of MTT, TU Delft
Committee Member:	Dr.ir. Marcel J.M. Hermans, Department of MSE, TU Delft

TU Delft
Department of Material Science and Engineering
Faculty Mechanical Engineering

Abstract

Micro-indentation testing has shown great promise in extracting local mechanical properties of ductile metal materials. Although the relevant contact physics has been well revealed since the 19th century, interpreting the indentation data still poses many challenges at the application level. Regarding one of the mainstream methodologies for extracting metal's representative stress-stain curve, the semi-analytical method has demonstrated remarkable performance towards the well-defined contact system involved. However, applying such a model to other indentation scenarios tends to cause some practical measuring problems. The validity of the results depends heavily on the practical experimental setup and the hardware testing calibration, which is inherently related to its accomplishment level in capturing the entire mechanical response. This thesis investigates such practical issues through a provided semi-analytical model validation. In addition, to capture a material's elastic modulus with less reliance on initial data, a novel analytical model has been proposed, with a special focus on the extensive unloading/reloading data.

However, both the analytical and semi-analytical methods are not fully applicable. For the analytical model, the first unloading segment contributes the most matched estimates of effective modulus to the tensile reference value, with an average deviation error of 6 %. But there still remain relatively large discrepancies between two similar samples. Besides, the validity of its results highly depends on accurate profile radius determination, which demands a more precise profilometry system. For the semi-analytical model validation, the resulting indentation strain-stress curves appear to exhibit post-yield behavior and fail to capture the effective modulus as well as the yield strength. It reveals the model's performance that heavily relies on the initial elastic data.

Acknowledgements

First of all, I would like to thank Dr. Vera Popvich for providing me with such an interesting master's thesis topic and coordinating the entire thesis project. I have benefited a lot from your prompt feedback and your working style that efficiently resolves issues requiring external consultation (such as questions related to the plastometer instrument). Additionally, I could feel your kindness and warm care when I got stuck at some point, which has brought me great encouragement. I am very glad to have the working experience with you.

Following is a very special thanks to my daily supervisor Niels Troost, for your guiding me through the entire thesis process with great patience. Your meticulous and pragmatic working attitude, as demonstrated by your convincing comments on my draft thesis report, has inspired me a lot and made me conduct the thesis with great determination and enthusiasm. Thanks to your laying a very clear and organized framework before, I quickly got acquainted with the study field during the initial stage of the project. I am also very grateful for your consistently offering patient explanations for my confusion, promptly steering me away from unnecessary explorations, and your well-considered suggestions for my writing in the literature review and experimental part summary. All of these significantly contribute to the completion of the thesis. Particularly for me, I am very impressed by your logical, patient, and friendly communication style, especially in your showing empathy which makes me quickly understand your perspectives. It has inspired me to put more effort into clear English communication further, and you have served as an excellent role model for my learning journey.

Further gratitude is given to Dr. Ton Riemslag, Elise Reinton, DP Mainali, and student assistants who have ever generously provided help with the experimental setups in the mechanical behavior lab and sample preparation lab. And finally, I would like to express my deepest gratitude to my wise parents and my dear boyfriend Liyan, for their love, allowing me to pursue my goals of exploring the world in science as well as my self-define.

Qinyi Zheng
Delft, the Netherlands
February 20, 2024

Contents

List of Figures

List of Tables

Chapter 1

Introduction

1.1 Indentation-based mechanical characterization

Indentation-based characterization, aimed at extracting local mechanical properties of materials, has significantly broadened its application scope in material science. This is particularly notable in fields such as additive manufacturing, pipeline materials, and welding materials, where conventional tensile tests may not always be feasible. For instance, in the friction stir welding industry, assessing joint strength is crucial for evaluating the manufacturing process and the related microstructure study. However, conventional uniaxial tensile tests face challenges in quantifying joint strength as they mainly focus on the weakest part of the testing specimen, which in the case of friction stir welded steel, tends to be the base material rather than the joint. Accordingly, the tensile tests primarily output mechanical properties of the base material, rather than providing insights specifically about the joint.

To study the static strength of the welding joint, one of the research interests is to address the microstructural evolution and mechanical properties of sort of welding zones at the micro or mesoscale level. Yet the latter has become a setback due to the constraints of relevant characterization techniques. Traditional local characterization methods highly rely on sample preparation to accurately simulate the thermal or mechanical history of the testing region. However, there remain doubts regarding whether the simulated sample material truly reflects the properties of the testing region. Theoretically, it is supposed never to reproduce the actual state of one another. The indentation technique is developed based on the localized mechanical response of the sampled material, achieved by simply pressing the indenter onto the target area. This provides an ideal solution to address the aforementioned sample simulation challenge, resulting in a more convenient and efficient testing procedure.

The working principle of the broadly defined indentation test mainly involved two aspects: indentation response capture (data collection) and data conversion. In the former case, the indentation response is typically captured and recorded by the instrument as applied load and indenter displacement data. The applied load indicates the stress level within the testing region, while the corresponding displacement represents the height change of the material-indenter contact region along the loading direction. This information effectively

reveals the deformed state of the penetrated material during indentation. Meanwhile, such instrument load-displacement(depth) data usually contains the elastic and plastic behavior of the penetrated material. This serves as a theoretical foundation supporting future data conversion for extracting elasticity and plasticity parameters.

1.2 Methodologies involved in data conversion and problem statements

With regard to indentation data conversion, there are two mainstream methodologies addressed in recent years along with two kinds of indentation data, according to the literature study: one depends on the semi-analytical way that mainly uses the instrument load-displacement data, and the other is named the "Inverse Finite Element Modelling (IFEM)" method, where both load-displacement data and residual profile data are commonly applied.

As for the former semi-analytical method, its effectiveness mainly depends on how to develop and optimize the contact model that accurately represents the relationship between stress (referred to as "load") in the contact region and the corresponding deformation along the loading direction (referred to as "displacement"). To align with the terminology "stress" and "strain" used in conventional tensile test curves, its data post-processing aims to interpret load-displacement data into an equivalent stress/strain curve for normalization. By integrating advanced numerical techniques like the Finite Element Method, it becomes feasible to reveal more comprehensive details about the entire contact process and iteratively refine sophisticated models across various contact system scenarios. However, this approach raises concerns regarding the model's applicability in specific practical scenarios, as well as the accuracy maintenance. Although the relevant physics have been well disclosed and widely accepted for a long time, which can even date back to the contact theory published by Hertz in 1896, applying this model to specific indentation scenarios still presents a lot of challenges. For example, testing different material categories, adopting different indenter geometries, and even the hardware testing system might significantly affect the outcomes.

Another type of indentation data, known as residual indent profile, commonly employed in the methodology of IFEM, offers an alternative perspective on indentation data conversion. Inspired by the uniform hardness test, this method takes a special focus on the permanent deformation of the material when penetrated by a harder material (indenter) with a specific load pattern. The material's resistance can be quantified and used to infer its plastic properties. However, because this approach primarily focuses on the material's permanent deformation after a single indentation test, it may not effectively reveal elastic information about the material.

In analyzing the entire process of spherical indentation, it can be determined that the contact surface of the material always reproduces the same spherical shape as the indenter bottom throughout the loading process. Upon unloading, the material surface undergoes

elastic recovery, transitioning from the original spherical deformed state to what we observe in the residual indent profile. Thus, the initial and final states of the material's elastic deformation can be determined, and through studying these two states, it may be feasible to obtain the material's elastic properties.

1.3 Structure of the thesis report

In this thesis, two research topics were conducted regarding the methodologies involved in indentation data conversion. The first one focuses on validating a provided semi-analytical model. It aims to investigate the model's adaptability to our in-house indentation test system and the sample material of DH36 steel, which is commonly used as the friction stir welding base material. In addition, some encountered measuring issues are also addressed when applying the model to the hardware measurement system in practice, such as the choice of indenter, the load pattern setting, and so on. This is expected to be meaningful for enhancing the practicality of the semi-analytical model. Relevant content can be found in Chapter 3.

The second part of our work, inspired by the features of residual indent data, involves a proposed method that extracts the material's elastic modulus through its unloading/reloading responses with the additional aid of profilometry. Specifically, this research emphasizes two major aspects: establishing the analytical model and designing practical experiments for model validation. This is expected to conduct some preliminary exploratory work on extracting the material's elastic property through the combination of load-displacement data and residual indent profile data. Relevant content can be found in Chapter 4.

The theoretical background and application context of the aforementioned work are detailed in the literature review part of Chapter 2. Conclusions and further recommendations are provided in Chapter 5. The main objective of the thesis is to gain insight into novel indentation-based local characterization, encompassing the study of its physical fundamentals and exploration of practical perspectives when integrated with specific applications.

Chapter 2

Literature Review

2.1 Application Background in Friction Stir Welding of Steel

Friction stir welding came into the historic picture relatively late in 1991 [1], primarily in response to tackling the joining problem of reputedly un-weldable aluminum alloys at that time. It utilizes the rotation of an un-consumable stir tool around the interface of two separated pieces and a coalescence is thus formed by the flow of the materials within the proper rational speed and transverse speed of the tool. The process is exothermic, and hence the localized heating materials near the joint line are softened and easily to be extruded by the movement of the stir tool, making them undergo intense plastic deformation at elevated temperatures. It should be noted that the heating temperature is expected never to reach the melting point of the working pieces, which ensures it is a so-called solid-state process.

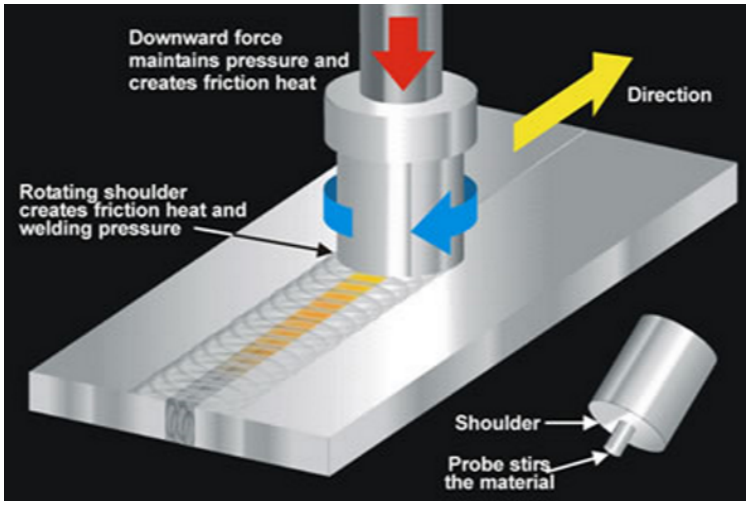

Figure 2.1: A visual representation showing the friction stir welding process and the stir tool involved in[2].

Since steel has always been dominant in engineering and construction materials by far,

it is undisputed and inspiring that many explorations of its applicability to steel have been reported. Compared to conventional fusion welding, shielding gas or flux is not necessarily involved in the FSW process, which delivers three general benefits[3]:

1. no concern for the compatibility between the welding metal and the flux or the cover gas.
2. Save more energy.
3. and the overall process of FSW is more environmentally friendly.

Besides, in the categories of Friction Welding, FSW is also notable for its great versatility in that it could be applied in various types of joints like butt joints, lap joints, and T butt joints[3].

Furthermore, many examples[4][5][6][7][8] show the static strength of the welding joint can be remarkably improved through the process, or in other words, it is much larger than that of the parent material. This is confirmed by typical fracture locations of FSW samples that failure usually occurs in the parent metal quite away from the joint. It also indicates, however, that the static strength of the steel FSW joint may be difficult to quantify by the conventional tensile tests, particularly when the welding process is carried out on two different base materials.

Figure 2.2: The positions where fractures occur in friction stir welded joints of AA7075-T6: (a) advancing side, (b) retreating side [7]

To study the static strength property of the FSW joint, typically it is highlighted in the literature about the relevant joining process along with their microstructural evolution. But following my investigation, the objective of most reported articles is to study how the bulk properties are influenced by the combined effects of welding parameters in the joining process, or how the bulk properties relate to the formation of the welding zones which are categorized by different levels of thermal cycle and plastic deformation (if possible) they are undergoing. The bulk properties here represent the weakest part of the entire specimen body which usually includes the base material and the joint. Even if the specimen is acquired merely from the welding joint, it still involves the contribution of all the welding zones as

the characterization is on the basis of whole-body measurement, like the way of uniaxial tensile test and fracture test.

The FSW technique has been developed for just a few decades, and most of the FSW-material-related research still targets the basic metallurgical examination within its joint area. For instance, the microstructural changes of each welding zone are normally analyzed from the literature, but there are not too many reports that step further to study how the welding parameters influence each highlighted welding zone (mainly for the nugget zone) in terms of their mechanical response, like the yield strength and work hardening behavior rather than simply their hardness values (which are seen as the semiquantitative indicators of the resistance to plastic deformation[9]). The main reason is due to the limit of the characterization method.

In the following section, a novel indentation characterization for local mechanical properties will be mainly introduced, in response to extending the local characterization technique for FSW joint and thus help establish its static strength-welding parameter relations with regard to this specific material. This technique provides critical mechanical property data of material by the combination of testing hardware with analytical techniques or advanced software solutions, which enables the measurement far more efficiently than conventional methods, and accordingly is considered the next generation for mechanical testing.

2.2 Indentation Technique for Local Strength

2.2.1 Comparison with normal local characterization

In analogy to the Wooden Bucket Theory[10], the bulk property of the material usually depends on its weakest area in mechanics. Therefore most mechanical tests are set up to mainly diagnose the weakest part of material like the tensile test. Under the research background of FSW, the static strength of the joint in steel is usually higher than that of the base materials. This would result in a complex characterization of the static strength of the joint, particularly when the FSW process involves two different base materials. Besides, in some cases material's mechanical properties in specific areas are also of great interest in scientific research. Take the example of the FSW joint part. It still remains unclear how each of the distinctive zones in the weld area is affected by this complex thermo-mechanical processing, where the welding parameters make a great difference. Due to the fact that these regions are characterized by different thermal and mechanical exposures, their mechanical behaviors are expected to vary from region to region at the micro-scale. Therefore, it raises a critical need to develop local mechanical testing with good accuracy and precision for further research.

There are two general approaches to testing mechanical properties at a small scale on the basis of conventional methods. The first one depends on the small size of the sampled material and this extracted size could be regarded as representative of the bulk. Take the sub-scale tensile tests as an example, typically the length scale of a micro-sample is around

a few millimeters[11]. The main testing challenges lie in the determination of the specimen's geometry and size and the preparation of them. For the FSW joint case, it seems unattainable to capture the mechanical response of each material zone since the regions are usually at the micro-scale. The second method, which is principally on the basis of processing simulation, is much more common in the field of welded joint analysis. Specifically, a comprehensive analysis is first made of the thermal and mechanical history of different welding zones. This leads to a well-simulated specimen that approximates the true situation in the local region. Conventional methods like uniaxial tensile testing are further carried out to gain its mechanical characteristics. However, it still remains some doubts about the reliability of the mechanical properties in different welding zones. First of all, the simulated processing for samples is not exactly equivalent to reality, and owing to the complexity of the thermal-mechanical process the accuracy of the simulation is hard to prove. Secondly, even if we pick up a perfect sampled material, it can not be avoided introducing external measurement errors within the tests themselves. For instance, the impact experiment requires specimens with standard notches causing additional local stress effects, and thereby the measurement results can not guarantee an actual impact strength of the simulated zone. This influence, sometimes, should not be underestimated for a process-simulated sample. In addition, whether the utilized sample can be a representative element of the bulk is theoretically with reservation. For example, the stress state, by principle, differs from in an individual sample and in the case when the sampled part acts as a component in a bulk. Obviously, this difference is larger when adopting general mechanical testings since they usually ignore the effect from the surrounding field of the picked zone. Besides, it is easy to imagine that the procedure for the sample preparation is considerably time-consuming by the conventional means, which significantly limits its wide application in local characterization.

The highlighted indentation-based technique, on the contrary, greatly simplifies the testing procedure with fairly easier and crude surface preparation of the sampled material. By combining the practical indentation tests with mathematical analysis or modeling learning, this technique has been proven a promising prospect by making the generated material property data accurate, reliable, and easy to acquire. These will be addressed in the following sections.

2.2.2 Hardware issues for collecting indentation data

The broadly defined indentation test, as the name suggests, relies on the simple operation of pushing a hard indenter into a sample surface. One of our best-known examples may be the universal hardness test. The application of the hardness test enables us to evaluate the resistance of one testing material to permanent deformation, by measuring the depth of indenter penetration or measuring the size of the indentation impression left by the indenter[12]. However, the obtained experiment result, the hardness value, is not a fundamental property of a material but only serves as the semi-quantitative indicator of the material's resistance to plastic deformation under the specific testing condition. Inspiringly, a step fur-

ther is taken to make it possible to acquire the material's mechanical property based on the indentation test, and this leads to a more ingenious experimental design and a more comprehensive analysis of the indentation response.

First of all, some considerations have given rise to some measurable issues, such as how to determine the size of the indenter and how deep it penetrates. This is because those concerns are closely tied to the physical nature of the material's mechanical behavior. In principle, local mechanical properties are set up through its analogous mechanical response from a homogeneous bulk. Thus the inherent attribute of local characterization also refers to the bulk one. Normally, to reveal the mechanical properties of the testing region, it requires the deformed region must be large enough that could be representative of the bulk. For the majority of polycrystalline (metallic) materials, their mechanical properties tightly depend on their grain structure at the micro-scale. There is a wide recognition[13] of a strategic point where the indent depth should be at least of the grain size order and the indent area is at least ten times the average grain size. The typical grain size is usually in the range of a few tens of microns, and this led to the minimum indent depths of this order and the minimum indenter diameter of hundreds of microns.

Particularly, there is a special demand for extracting materials' plasticity characteristics. Normally, in order to obtain a reliable plasticity measurement, the testing material must undergo deformations of at least 15 to 20% in strain[13][14]. The extent of strain produced during indentation primarily relies on the penetration ratio, which is the ratio between the penetration depth and the indenter radius. The penetration ratio in the indentation test is considered acceptable, for obtaining material's plasticity information, only if it generates much more strains of this magnitude. In practical applications when using profilometry data, this can be realized by employing an indenter with diameters of the order of 1mm with a penetration ratio of 20-25% as a sort of compromise value[13], for example. The loading magnitudes usually vary in the type of material but may not be far more than the KN range. It should be noted that the nanoindentation technique which possesses a finer nanoscale testing resolution can not be applied to extract material's plasticity properties, rigorously. This is because the maximum loads applied by a nanoindenter, typically only a few tens of Newtons, are insufficient to create a representative plastically deformed volume[9].

Furthermore, the choice of indenter geometry may also have an impact on the final outcomes. According to the literature study, it usually depends on several underlying aspects that are not limited to the property of the testing material, the test objective, or even the type of method adopted for data post-processing. For example, it is much preferred to apply spherical indenters to extract the plasticity characteristics from instrumented indentation data, as highlighted in the reported novel approach[15]. The author pointed out the significance of the spherical geometry owing to its non-self-similar feature. This provides a dynamic strain field for indentation that the strain field always changes with increasing penetration depth and thus gives extra degrees of freedom that enhance the convergence in the inference method (relevant introduction about the approach will be given in Section 3.5.2). The motivation behind each choice varies from case to case and it is not feasible to

elaborate it due to the space limitation.

After the indentation is carried out on a sample surface with a specific indenter, the corresponding indentation response becomes the main research subject for determining material's mechanical properties. The indentation data could either be the load-displacement plot, or the residual indent profile, which is evaluated as a crucial representation of material's response to indentation. While the indentation responses, inherently, can be owing to the unique elastic and plastic deformation within the testing material. Therefore, Young's modulus (elasticity parameters), yield strength, and work-hardening behavior (plasticity parameters) become underlying properties to describe the indentation response. Conversely, it can be concluded material's indentation response is able to reflect its general mechanical properties, either in elasticity or plasticity. To well explain it, the following section turns to the mechanisms of material's elastic and plastic behavior firstly, from which perspective this enables the foundation of meaningful and reliable insights in further data analysis/conversion, and finally the extraction of the static strength property for the penetrating material.

2.2.3 Material's elastic and plastic behavior

A material's elastic behavior refers to its capability of "reversible" deformation to resist the applied load. In other words, when stress is applied to the material, it temporarily changes its initial shape and size and returns to its original form after the applied stress is removed. It indicates the material is under elastic deformation. This is in contrast to plastic deformation, in which case the material fails to return back after load removal and remains in its deformed state permanently. The elastic behavior is typically described using the property of Young's modulus, which is measured as the ratio of stress (force per unit area) and strain (relative deformation) within the elastic limit of a material when subjected to adequate load.

Apart from the elastic deformation, the indentation testing procedure also involves the plastic deformation of the material if the stress exceeds the point of so-called yield stress or yield strength of the material(relevant introduction of yield strength is present in 1). Normally, the plastic deformation can be well expressed through its "hardening" ("strengthening") behavior and this is in analogy with the "post-yield" part of the stress-strain curve obtained from uniaxial tensile testing. Unlike the simple quantification method in elasticity or simply the determination of yield strength, it is much more complicated to quantify or interpret how a material behaves under plastic deformation. This is mainly due to its more complex inner-behavior mechanism when responding to external forces.

"Hardening" or "strengthening" can be understood by taking it literally to describe what happens inside the material: the necessary deviatoric stress increases progressively to maintain the plastic deformation and allow the straining to continue. In a true stress-strain curve(as shown in2.3), this behavior refers to the subsequent rise of true stress with true strain after the yield point, and the slope of this so-called hardening curve is the work-

hardening coefficient or hardening rate. It is worth noting that hardening curves vary considerably in different materials or at different deformation states. And this could be mainly explained by several mechanisms studying how the movement of dislocation is hindered (other processes can also be involved in plastic deformation, such as diffusion and deformation twining), ranging from solid solution hardening, dispersion hardening, precipitation hardening, grain refinement and so on. In essence, it usually comes into being via interacting with other dislocations, generating new dislocations or increasing grain boundaries. But generally, the hardening rate tends to decrease less and less and perhaps eventually approach a constant value (i.e. approach the equilibrium state). This is a consequence of competition between the physical hardening (quantified as the hardening rate) and the geometrical softening (quantified as the reduction rate of the cross-section), which in turn determines the stability of plastic deformation. Besides, it can also be attributed to the combined effect when new dislocations are generated, their mobility begins to be suppressed, while some confrontational processes (like climb or cross-slip) take place to promote dislocation with a smooth motion.

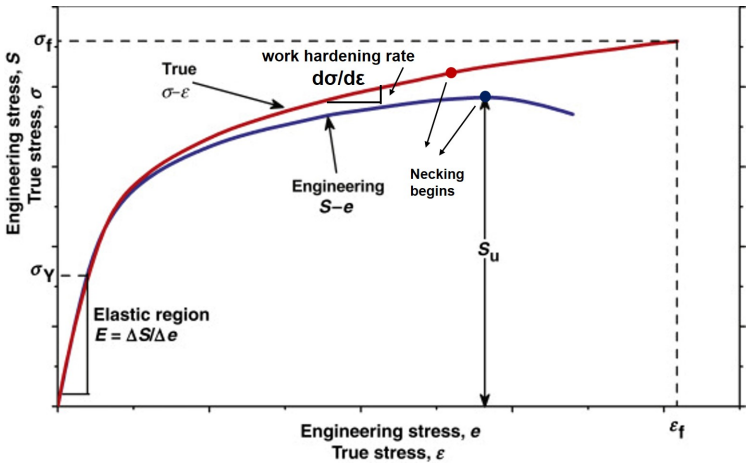

Figure 2.3: Typical monotonic stress-strain curve[16]

To visualize the hardening behavior, it can somewhat be analytically expressed in a constitutive law for ductile metal. Of course, compared with the characterization of elasticity, it is more complicated. Therewith several analytical expressions are proposed to conform the real work hardening curve as close as possible, but only two of them are in common use. The first one is the Ludwik-Hollomon equation:

$$\sigma = \sigma_y + K\varepsilon^n \tag{2.1}$$

Where σ is the applied stress (Von Mises stress), ε is the plastic strain (Von Mises strain), σ_y is the value at yield point, K is the work hardening coefficient or the hardening rate, and n is the work hardening exponent.
The other is the Voce equation, as shown below:

$$\sigma = \sigma_s - (\sigma_s - \sigma_y)e^{-\varepsilon/\varepsilon_0} \tag{2.2}$$

Here σ_s represents a saturation level, and ε_0 is a characteristic strain when the corresponding stress approaches the exponential level of σ_s. With no doubt, a wide variety of hardening curves can be obtained by manipulating the above parameters analytically. And the highlighted constitutive laws are the basis for the global activity in FEM simulating the progressive plastic deformation in metals.

To sum up, material's mechanical response due to indentation can be fundamentally characterized as a combination of elastic and plastic behavior, and both of them can be quantified, compared, and utilized to describe the properties of materials. For instance, elasticity can reflect a material's stiffness, the initiation of plastic deformation can be expressed as a material's yield strength characteristic, and work hardening parameters from the constitutive law can be employed to describe material's hardening behavior while undergoing plastic deformation. It should also be noted that the indentation response of a material consists of both elastic and plastic responses, which can be in analogy with what happened during the uniaxial tensile test. It provides a theoretical justification for the conversion from the indentation test results to material's mechanical properties we normally know. The following sections will dive into the indentation data conversion part, taking one of the most popular methods — the Inverse Finite Element Modelling (IFEM) as the main study object to discuss the practical conversion issues for extracting material's mechanical properties.

2.3 Indentation data conversion

After capturing the indentation responses and collecting them as indentation data, it raises an issue with the data post-process that converts the indentation data into the normally-known mechanical properties, such as Young's modulus, and yield strength. Generally, there are two mainstream approaches in current research studies: Inverse Finite Element Modeling (IFEM) and the semi-analytical method. In essence, both of them are built on modeling learning or "transfer learning[17]". The IFEM method, as the name suggests, primarily relies on the database of indentation simulation created through Finite Element Modelling (FEM) before entering into the inversing part. In this case, it utilizes the pre-trained indentation models and treats it as an initialization problem for addressing the diverse contact problem in practice. While the latter semi-analytical method is conducted as a kind of feature analysis from one existing contact model between the indenter and sample surface. Thus this can also be considered a form of "transfer learning" and the applicability of the contact model should be taken into great account.

To be specific, in the context of IFEM method, the practical measurements of indentation response are set aligned to the modeled results derived from the FEM simulations, and mechanical properties of actual testing material can be then acquired by the alignment with the FEM database. Therefore, to maintain the accuracy of this method, two critical factors must be taken into consideration. First, a large enough material database must be created

beforehand to ensure a representative diversity of indentation responses, and secondly, there should be a careful selection of the formulations embedded in the FEM model that involves appropriate property parameters, which can effectively capture the real response of a cross-section of material during uniaxial tensile tests.

In terms of the semi-analytical approach, primarily, its objective target is to seek the appropriate mathematical expressions that reflect the underlying principles from the contact model, either through the analytical or the numerical way (this will be elaborated in further section 3.5.1). For instance, one of the critical analytical expressions can be the relationship between indentation load (P) and indentation elastic displacement (h_e), derived from Hertz's model[reference!!!]. In addition, stress and strain appearing or defined in the conventional tensile test should be carefully reviewed when regarding the indentation test, and this is due to the fact that the testing specimens are under different loading systems in the two cases (tensile force for the former and compressed one for the latter). It inspires us to figure out the essence of "stress " or "strain" before constructing the equivalent stress-strain curve to estimate the properties of the testing material. Hence, to maintain the accuracy of this method, several factors need to be addressed, including but not limited to the adaptability of the contact model; the validity of the analytical mathematical expressions; the effectiveness of the new definitions for substituting the items that peculiar to the conventional tensile test (such as the definition of indentation stress/strain or indentation yield strength), and so on. Apparently, this method involves many more factors that influence the credibility of the final results in comparison to the IFEM method.

Moreover, as reported in the literature[18], the latter IFEM method is seen as performing better in capturing plasticity parameters of metallic ductile material due to its involvement of the constitutive laws that characterize the work hardening of metals additionally. In this regard, the subsequent subsection takes a special focus on comparing the two methodologies, both of which utilize load-displacement curves as the sole type of indentation data for the "translation" of material's mechanical properties. The main objective of this subsection is to offer a more specific elucidation of the distinctive characteristics inherent in each of the two methodologies.

2.3.1 Load-displacement case

Preliminary, this case usually appeared in the primary study of the "Instrumented Indentation Technique (IIT)" on the basis of some analytical relations. The "instrumented" suggests that raw data like the applied force, and displacement will be measured for the entire time once the indenter is detected contacting the sample surface. Specifically, there are several segments involved in one loading-unloading cycle test, as follows:

1) When approaching the sample surface, the indenter is pressed into the sample material with a multi-step increase in applied force or penetration until the maximum is achieved. The terminal point for one loading depends on the given indentation mode, whether it is force-controlled or displacement-controlled.

2) The peak force applied on the indenter is then kept constant for a setting dwell time (usually for 5-10 seconds).

3) The load on the indenter will be gradually released within a user-specified rate (which is commonly comparable to the loading rate) until the force reach a small percentage of the maximum force, usually 10%.

4) The force on the indenter is also kept constant for a dwell time at this bottom. Both the dwell time during peak force and bottom force aim at reducing the so-called "thermal drift" effect which inevitably caused by the thermal expansion and contraction of the machine and/or testing material.

5) Those raw measurements are then put into the calculation channels of contact force (P) and penetration depth (h) where other influence factors such as originating from machine compliance and environment will also be taken into consideration[19].

The above shows the general practical measurement to gain this specific indentation data. It will then be converted into some of material's mechanical properties through either the semi-analytical way or the IFEM method.

2.3.1.1 In semi-analytical way

In the semi-analytical method, the collected load-displacement data is processed by combining both analytical (exact mathematical solutions) and numerical (approximate solutions using computational methods) techniques and employed to assess the properties such as hardness, elastic modulus, and other mechanical characteristics of materials. As for the former elasticity property, its analysis is mostly on the basis of elastic contact mechanics originally proposed by Hertz[20] that the elastic part of an indentation can be taken as the contact problem between two spheres with different radii and elastic constants. Some relevant equations were then derived for this specific case of spherical contacts, but they couldn't be directly applied to other shapes or more complex contact situations. In this respect, many studies were engaged to extend the contact theory and it has to mention the contribution of Tabor that he made a great analysis advancement from his experimental work in which the load-displacement curve was mainly analyzed for some mechanical properties[21][22]. One of the inspirations from his work extends Hertz's model to the contact with a non-rigid indenter, and he subtly included the indenter's effect on the indentation behavior by defining a so-called reduced modulus E_r that counts the elastic information (Young's modulus E and Poisson ratio υ) both of the sample and the indenter, through the equation:

$$\frac{1}{E_r} = \frac{1-\upsilon^2}{E} + \frac{1-\upsilon_i^2}{E_i} \tag{2.3}$$

Here, the subscripts i and s refer to the indenter and sample, respectively.

The reduced modulus was more effectively related to indentation load-displacement data subsequently through the analysis work by Bulychev, Alekhin, Shorshorov, and so on[23]. The reduced modulus can be calculated from the equation below:

$$E_r = \frac{\sqrt{\pi}}{2}\frac{S}{\sqrt{A}} \tag{2.4}$$

Where A is the contact area and is calculated as a function of contact depth h_c(as shown in Figure 2.4 depending on the indenter geometry and testing scale. In particular for indenters with the geometry of pyramid, cone, or sphere, the contact depth can be directly calculated through the equation below, linking to the total depth h, applied load P, according to "Oliver-Pharr model[23]":

$$h_c = h - 0.75\frac{P}{S} \tag{2.5}$$

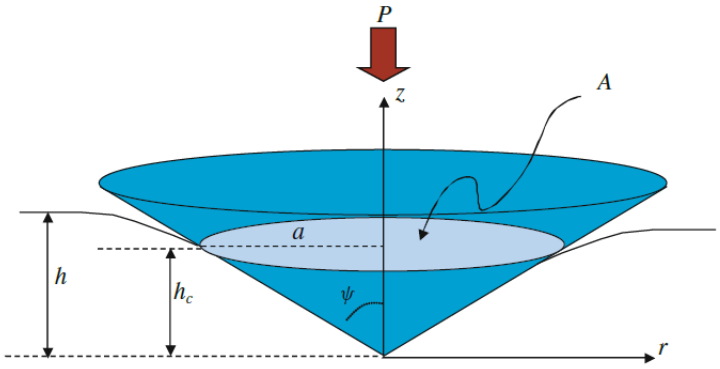

Figure 2.4: Schematic illustration of an indentation test[19]

In both equations 2.4, 2.5, S is called contact stiffness or the elastic stiffness of the contact. It can be gained from the upper portion of the first unloading data in the load-displacement curve (usually above 50% of the maximum force). Specifically, S is determined by fitting the mentioned unloading data to the expression of the form below:

$$P = B(h - h_f)^m \tag{2.6}$$

Where P and h are the given measurement data force and displacement, respectively. B, h_f , and m are best-fit constants to be figured out. Once they have been determined, S is able to be evaluated at the maximum displacement, as shown below:

$$S = \left.\frac{dP}{dh}\right|_{h=h_{max}} = Bm(h_{max} - h_f)^{m-1} \tag{2.7}$$

Therefore, the contact length and area can also be determined with a definite S and so does the reduced modulus. Young's modulus can thus be calculated from the variant of the equation 2.3:

$$E = (1-\upsilon^2)[\frac{1}{E_r} - \frac{1-\upsilon_i^2}{E_i}]^{-1} \tag{2.8}$$

Hardness is calculated as:

$$H = \frac{P}{A} \tag{2.9}$$

Where P and A are respectively referred to the maximum load and the corresponding contact area which can be induced from the residual indentation area. Hardness is also seen as the mean pressure of the contact.

When it comes to including plasticity, the contact procedure becomes much more complicated while the generated stress and strain fields are considerably heterogeneous under the indenter. This can be manifested in the indentation curve. For instance, the analytical fitting equations of the load-displacement relation are not as simple as linear in the elastic part. A series of plasticity parameters are defined and involved to explain the material's indentation behavior, such as yield strength, elastic-plastic transition and work hardening behavior.

With respect to yield strength, most of the traditional methods employ the aforementioned hardness value H to quantify the resistance to plastic deformation of materials. For instance, Meyer[24] proposes that the onset of plastic deformation could be correlated with a specific hardness which is obtained in the limit of zero residual indent. It inspires the relation investigations between yield strength and particular hardness. Tabor[25] later reported a credible scaling factor of 2.8 for translating the hardness measurement via spherical indenter to tensile flow stress that is usually obtained in standardized tensile tests.

From another perspective, normally, yield strength is defined as the stress where a preset amount of permanent deformation occurs. (In most cases 0.2% is taken as the predetermined offset value, making the permanent strain always equal to the same remainder when subtracting the elastic strain from the preset value of 0.2%.) The point at yield in the indentation test can also be treated in the same way and follow the same essence of a predetermined amount of plastic deformation. In other words, there should be a logically equivalent definition of yield strength when employing an indentation test.

Of course, altering the definition tends to make a difference in the output of all the plasticity parameters.

Prior to the yield strength definition here, it is necessary to set up a representative stress-strain curve before capturing a yield point. In other words, the indentation strain and stress should be defined beforehand.

$$\sigma_{ind} = \frac{P}{\pi a^2} \tag{2.10}$$

$$\varepsilon_{ind} = \frac{4}{3\pi}\frac{h_t}{a} \tag{2.11}$$

For elastic part:

$$\sigma_{ind} = E_{ind}\varepsilon_{ind} \tag{2.12}$$

Equations above 2.20, 2.21, 2.22 are proposed a good example of indentation stress-strain clarification, in analogy to the elastic strain and stress described in Hertz' model (Hertz' model basically bases on the elastic contact between two linear isotropic elastic solids), the indentation strain is generalized by substituting the elastic depth h_e with the total depth h_t. a is the contact radius and h_t/a is related to deformation in terms of relative angular displacement(see the schematic 2.5). Indentation stress is calculated by dividing the indentation load by the contact surface. Indentation modulus E_{ind}, is also regarded as the reduced modulus E_r or effective modulus E_{eff}, taking account into Young's modulus of both contact subjects either the sampled material or the indenter.

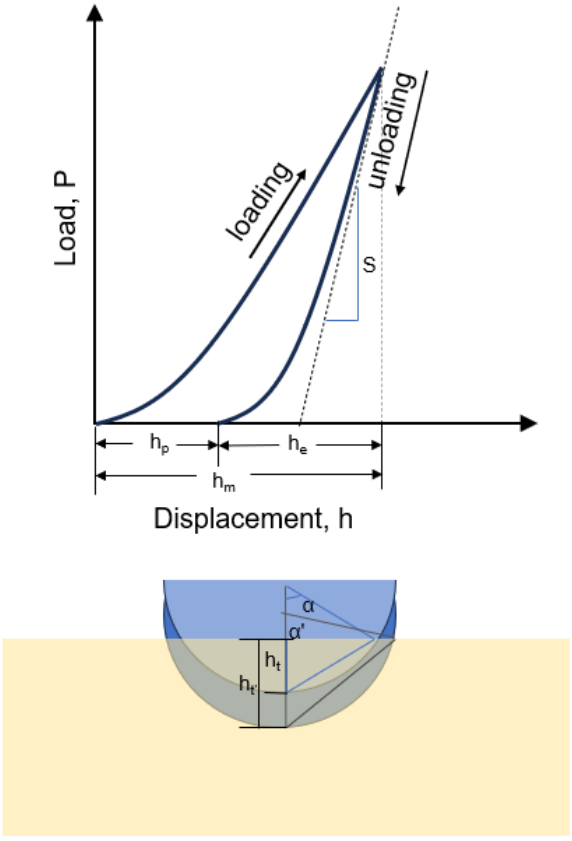

Figure 2.5: Schematic of one load step during indentation test and its corresponding measurement of the load-depth curve. Note: this schematic diagram is an original creation so no citation is shown up.

The referred article[26] from the Kalidindi group serves as a good example of extracting indentation modulus E_{ind} and indentation yield strength Y_{ind} based on a similar methodol-

ogy. In their study, the capture of elastic information is also based on the well-established Hertz theory, expressed as the equations below:

$$P = \frac{4}{3} E_{eff} R_{eff}^{\frac{1}{2}} h_e^{\frac{3}{2}} \tag{2.13}$$

$$a = \sqrt{R_{eff} h_e} \tag{2.14}$$

$$\frac{1}{R_{eff}} = \frac{1}{R_i} + \frac{1}{R_s} \tag{2.15}$$

Figure 2.6 demonstrates one of their research results. Their analysis of the raw P-h curve begins from the determination of a so-called 'effective zero-point' by removing some sort of initial noises (caused by some unavoidable factors such as the imperfect surface layer). It was accomplished by first fitting the initial elastic segment of the load-displacement(P-h) data to the variant of equations 2.28, 2.24 to estimate the effective indentation Young's modulus "E_{eff}"(it also called reduced modulus "E_r")(assume it is always the same), see the variant equations below.

$$h = k(P - P^*)^{\frac{2}{3}} + h^*, k = (\frac{4}{3} E_{eff})^{-\frac{2}{3}} R_{eff}^{-\frac{1}{3}} \tag{2.16}$$

$$a = \sqrt{R_{eff}(h - h^*)} \tag{2.17}$$

Here P^* and P^* demonstrate the load and displacement at zero point for the zero resets of original P-h data. In the initial point, R_{eff} is equal to R_i since the R_s approaches ∞ according to equation 2.15. Regarding each of the loading-unloading cycles, it is feasible that various R_{eff} can be obtained by following the same fitting rule used previously, where "E_{eff}" has already been known. In addition, the corresponding contact radius "a" can also be induced from the variant equation 2.24, in which case h_e can be acquired by the difference of the peak displacement and the residual displacement upon one complete unloading step. Hence, the indentation strain/stress (ISS) relation is able to be built by the equations 2.21, 2.20. An interesting finding from their work is related to the definition of the indentation strength Y_{ind}. They estimated the Y_{ind} using the 0.2% indentation strain offset line to intersect the fitting ISS curve in the strain range of 0.001 and 0.003. But it may raise a problem that Y_{ind} cannot be adequately captured, i.e. this intersection may be impossible with a blank zone of the fitting ISS data. Such an issue emerges commonly if the material has quite a great elastic-plastic transition zone that the indentation machine is not able to capture enough points near the indentation yield due to the limit of resolution.

To sum up, it is still quick and easy to obtain material properties by adopting the direct conversion from load-depth indentation data using a semi-analytical way. Most of the understanding work of an entire indentation curve could be realized through experimentation and finite element simulation. However, this approach is based on several concise equations

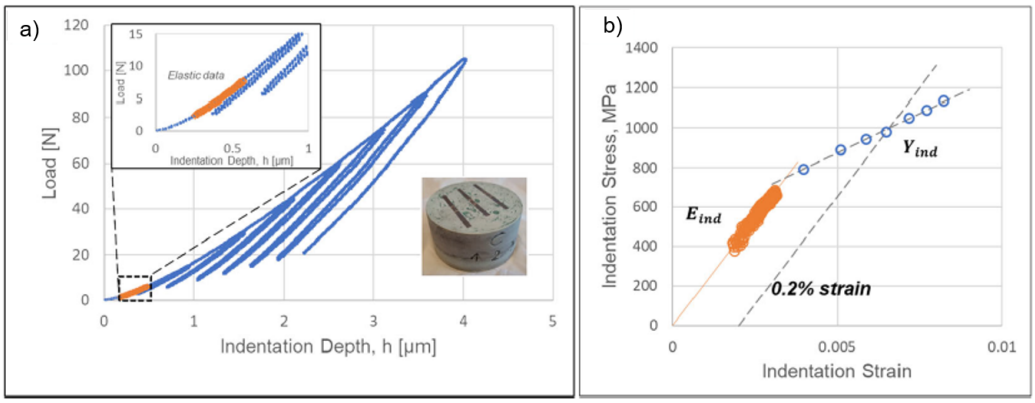

Figure 2.6: a) The load-displacement (P-h) curve obtained from the indentation test. Elastic data highlighted in orange was identified using the protocols described in the paper. b) The corresponding indentation stress-strain curve. The blue points are called the post-elastic data, each of which link to one sort of unloading-loading cycle[26]

and models involving gross simplifications in the contact procedure. Seeking a more accurate model is always the final target in this field while such a model usually varies in testing materials.

2.3.1.2 In IFEM

Material's mechanical behavior, as mentioned before, requires certain defined parameters for characterization. For instance, a material's plasticity behavior can be simply described using sets of Ludwik-Hollomon or Voce parameters in addition to its stress-strain curve. The material model is then parameterized in terms of these mechanical parameters. While inputting material parameters and the loading step, one can predict the corresponding indentation data by means of finite element modeling. Thus it is easy to create a material database containing a great amount of indentation responses from materials with definite mechanical properties. Inverse Finite Element Method (IFEM), on the contrary, works on the principle that it switches the input and output from the prior FEM case: under specific testing conditions, inputting a desired indentation response such as the load-displacement relation (often this is obtained from actual loading tests), and the model ensures a confidence output of the corresponding mechanical parameters of the testing material. This is realized through the use of a specific convergence algorithm for efficient scanning of parameter space, seeking an optimum parameter set within the database. The principle of IFEM can be well explained from the outline diagram 2.7 below. (Note, here in the Figure, a single indentation load-displacement data is taken as the indentation data for conversion. This Figure is the graphical abstract of article[15] found in the publish website.)

When importing the experimental load-displacement data as the input data for further

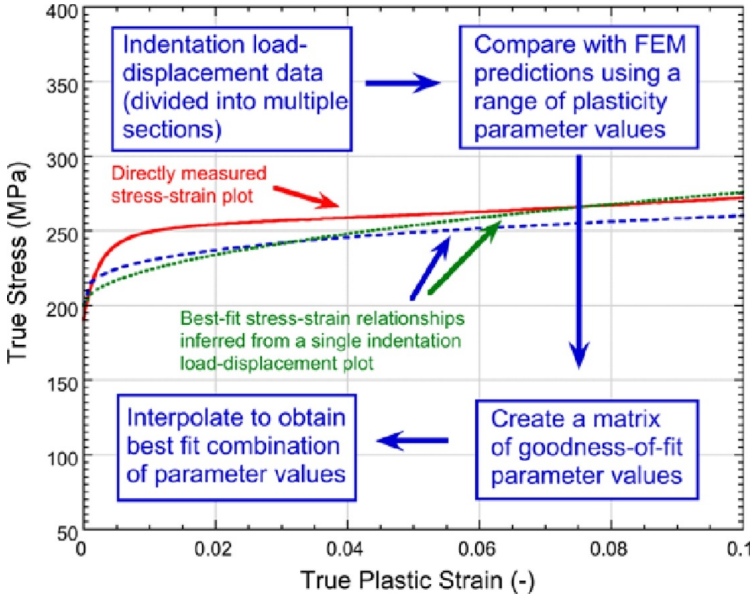

Figure 2.7: Overview of the IFEM method[15]

analysis in the IFEM method, the measured data is compared with the simulated indentation responses data from the pre-created indentation database. Once they reach a confidential agreement with each other, it suggests the modeled indentation procedure is considered in accordance with the actual indentation test where the imported load-displacement data comes from. Since there is no other great difference in the indentation procedure between the practice and the modeling one, their corresponding mechanical properties can be equated as the two indentation data reflect nearly identical elastic or plastic behaviors. The above is referred to as the inverse part of the input indentation data in IFEM.

However, there may raise some issues termed inverse problems. For example, it is likely to emerge errors during iterative simulation that more than one solution may be deduced if within an unnecessary compensation while scanning for an optimum parameter. One of the underlying causes lies in the complex characteristic parameters to be sought that they incorporate plenty of freedom degrees, ranging from the yield strength value, work hardening rate as a function of strain and so on. Such an issue, in principle, can be tackled by optimizing the relevant algorithm or the converging technique for a more efficient and accurate solution.

On the other hand, this can be also attributed to the low sensitivity of the input data (load-displacement plot in this case) towards the inference characteristics. Primarily, this is attributed to the poor resolution inherent in the experimental measurements. There always exists inevitable noise of the displacement data in the actual indentation test, as a consequence of the high perceptivity of the measuring tool to external factors, such as the frictional effects of the contact, surface roughness of the testing material, and the indenter imperfections, etc. In addition, it is also likely to cause some problems with machine com-

pliance in the loading(unloading) process, and this cannot be underestimated toward the instrumented indentation tests on hard material[27], such as the FSW steel to be studied.

Several studies have been focused on coping with these inverse problems, according to the reference[28]. Instead of simply broadening the number of hardware tests, many approaches have been developed to guarantee the simulated outcomes with high reliability and accuracy, and with fewer trials. The group of Pelletier[29] carried out the indentation tests using two different indenters, and it was confirmed that the acquired data yielded more precise estimations of Young's modulus, yield stress, and strain-hardening exponent due to their more different indentation responses have been captured. Besides, they also suggested that combining additional indentation data (such as residual indent shapes) inference would boost the sensitivity of experimental response to the constitutive relation.

It indicates the accuracy maintained in the IFEM approach mostly relies on two aspects. One is for the amount of mechanical responses the imported indentation data have contained. The other can be ascribed to the convergence stability between the measured load-displacement data and the modeled one. Therefore, to attain a high level of accuracy in extracting material properties, the imported indentation data plays a crucial role in addition to enhancing the algorithm in the inversing part. The input indentation data is not only required to avoid of excessive measurement noise that assists the convergence but is also supposed to contain plentiful enough mechanical responses, making it better in revealing the property of the testing material.

2.3.2 Residual indent profile case

Rather than the in-situ testing of load and displacement, measuring the residual indent profile serves as another good alternative for the indentation data to be applied in the IFEM method. Figure 2.8 is a typical example of such measurement where the radial distance and the corresponding height from the original sample surface are taken to quantify the indent profile.

There are certain advantages of the latter over the use of the load-displacement plot according to the literature study.

Firstly, it eases the measurement that the target is simply the final residual profile after indentation (i.e. static residual profile measurement). This saves a great amount of sensing time to reach the required high resolution since there is no need to monitor the instantaneous load/displacement during actual indentation except the last value of the load.

Secondly, it is also easier to implement a more accurate and rapid measurement when treating the residual profile as the target outcome. This can be realized merely by attaching some mechanical and optical profilometry techniques apart from the load system. Nowadays in the commercialization of Profilometry-based Indentation Plastometry (PIP) testing, the profilometer is usually designed based on the radially symmetric of the expected indent

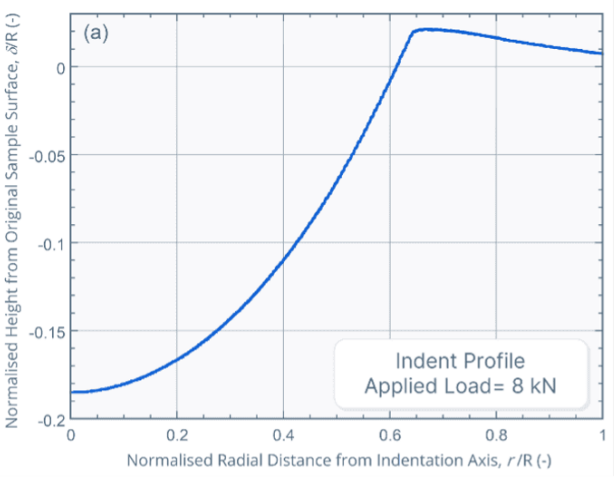

Figure 2.8: a residual indent profile data [30]

profile. The measurement accuracy can be simply guaranteed by averaging the profile data gained from two orthogonal scans[13](i.e. scanning the indentation in two perpendicular directions through the central axis of the indent). The averaged profile data is used to compare with the profile database for further analysis. It should be noted the residual profile monitor may not expect the sampled material to have any anisotropic behavior. There should be more than one resulting profile to represent the anisotropic responses rather than taking the average of two profile data of significant difference. In addition, the main error generated by the profile monitoring comes from the flatness level of the sample. Usually, this can be avoided by the embedded tilt correction function taking the scans of far-field parallel parts as the reference.

Besides, there is also the concern about the sensitivity when making a choice of indentation data in the IFEM method. The primary objective of this method is to enhance the efficiency of convergence on the best-fit parameter sets, plus to ensure their reliability in terms of capturing the material response. Article[13] has reported a theoretical investigation that the sensitivity issue can be well illustrated by the misfit parameter (S_{red}) distribution in the "goodness-of-fit" maps where simulated outcomes with various combinations of yield strength(σ_Y) and work hardening coefficient (K) are compared with a correct set of values($\sigma_{Y,true}$=245.6 MPa and K_{true}=102.9 MPa), as seen in Figure 2.9. In the four cases present, all of them demonstrate a "compensation" effect, i.e. if σ_Y is below the 'correct' value, it is possible to achieve reasonably good agreement by compensatorily increasing K, and the reverse holds true as well. In particular, the profilometry data case gives a more intensive range of the outcome, making it more sensitive towards the represented mechanical properties.

The dimensionless parameter (S_{red}), also called the "reduced sum of squares of the residuals", is commonly used in the convergence algorithm for a goodness-of-fit between

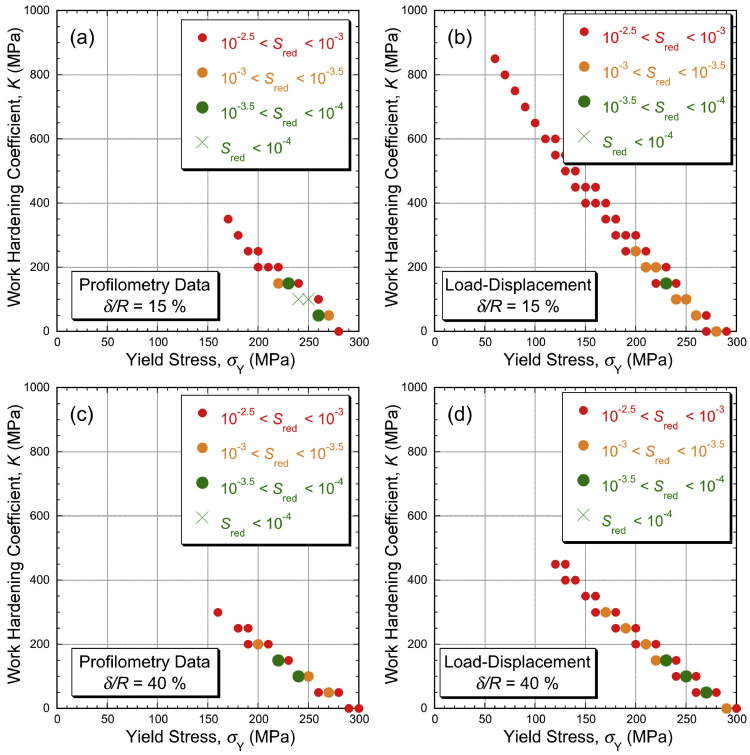

Figure 2.9: Goodness-of-fit maps for a low work hardening material (AR-Cu). It shows the S_{red} for various combinations of σ_Y and K in four cases: (a) penetration ratio δ/R at 15% penetration, using profilemetry data (b) penetration ratio δ/R at 15% penetration, using load-displacement data, (c)penetration ratio δ/R at 40% penetration, using profilemetry data, and (d) penetration ratio δ/R at 40% penetration, using load-displacement data.[13]

the target and modeled data with respect to the residual profile. Its expression can be normally expressed as:

$$S_{av} = \frac{\sum_N^{i=1} (\delta_{i,M} - \delta_{i,E})^2}{N} \tag{2.18}$$

$$S_{red} = \frac{\sum_N^{i=1} (\delta_{i,M} - \delta_{i,E})^2}{N\delta_{av,E}^2} \tag{2.19}$$

Here δ_i is the ith value of the height difference from the sample surface while subscripts M and E refer to the modeled data predicted by FEM and the experimental value. N is the total number of radial spaces being scanned and it primarily depends on the radial range and scanning intervals. It is apparent that a perfect fit also means the average squares of the residuals approaches zero.

Since S_{av} is dimensional, it has units and its magnitude cannot be used to give a universal indication of the quality of the fit. For this purpose, the above S_{av} is divided by the $\delta_{av,E}^2$,

namely, the numerical average of the maximum and minimum heights from the experiment data.

Nevertheless, utilizing the residual profile as the indentation data in IFEM could only obtain material's plasticity information since the convergence target is essentially on the basis of the constitutive law and it mainly regards plastic deformation. Elastic properties, such as Young's modulus or Poisson ratio, are prior to being set when creating the underlying FEM database. This is due to the fact that those input elastic parameters do not impact much on the inverse of plasticity parameters. Furthermore, to obtain material's property in terms of its entire mechanical response, further work is inspired to combine the two indentation data and make each of them do their best. This is not hard to understand since residual profile data enables IFEM a more rigorous scheme to gain material's plasticity parameter while the displacement data is good at capturing its elastic response.

2.4 Sample Effects on Indentation Characterization

2.4.1 A case study in PIP testing

To characterize one material's mechanical behavior, there may arise several points concerning sample preparation. Taking one of the commercial indentation tests Profilometry-based Indentation Plastometry (PIP) as the case study for this Chapter. Normally, a sample is treated by several surface preparation techniques before it is to be measured in the PIP test: cutting, grinding, polishing, etching, and so on. Each of these processes is possible to affect the indentation response of the near-surface region since PIP testing detects a relatively shallow layer, around hundreds of microns deep. For example, the grinding process may probably induce plastic deformation and cause some prior microstructural changes, ranging from the change in dislocation density, grain shape, grain boundary, texture, and so on. Samples with high initial work hardening rates are more sensitive for this condition as the process-induced changes can be further extended in the PIP testing[18]. However, as the manual of the Indentation Plastometer is given, virtually the surface requirement for the indentation plastometry is flat and relatively smooth, with a recommended finish for the treatment scale of a P2500 grit grind or finer. This is owing to its fairly large ratio of the penetration depth h or δ to the total scale of the sample's surface roughness plus contamination/oxide films. The latte factor makes only less than 10 μm thick of subsurface region be affected), and this is tolerant when carrying out PIP testing. The penetration ratio between the penetration depth and the indenter radius, δ/R, is normally specified as 20-25%[31], which ensures a fairly large testing area that is less affected by the potential coarse grain structure of sampled material. It thereby indicates a comparative cruder and simpler surface preparation. Nevertheless, it is meaningful to be aware of whether some relevant microstructural changes are caused and thus affect the PIP testing procedure, leading to unconvincing test results.

As a novel-developed mechanical characterization method, PIP testing is promisingly gifted with detecting some "sample-specific" factors, including but not limited to the pres-

ence of sample anisotropy, inhomogeneity, and local residual stresses. Superior to the conventional uniaxial tensile test or hardness test, this technique tends to give much more mechanical information with less effort in sample preparation.

2.4.1.1 Sample anisotropy effect

A sample is considered anisotropic if it has varied responses when loaded in different directions. For single crystals, it accounts for the discrepancy between the crystal orientation and loading axis that leads to different slip systems operations. When it comes to polycrystalline metallic samples, sample anisotropy generally attribute to "texture" where the grain orientations prefer some certain direction(s), or in other words they are distributed non-randomly. Similar to a single crystal, the textured material also exhibits its anisotropy when the loading axis changes. The purpose of studying material anisotropy is to figure out the underlying mechanism involved in the multiaxial deformation and this results in a more reliable and complete local characterization of materials. In PIP testing, such anisotropic information can be well elaborated through their corresponding stress-strain curves rather than a hardness value. Besides, the anisotropic information can be acquired by cutting the sample material at various angles to make different indentation axes. This is much more convenient than testing anisotropy in uniaxial tests because it is not always easy to prepare several anisotropic specimens in one bulk material.

2.4.1.2 Residual stress effect

In general, there is hardly any issue with the residual stress in conventional uniaxial testing. It is due to the fact that the entire volume of the material counts for the obtained mechanical behavior while all the residual stress must sum to zero and hardly make any difference on the whole. However, as for local characterization, residual stress needs to be specially taken into account because it can reach a high level and even above the yield stress of the material. During the indentation test, primarily, an indenter creates compressive stress close to the penetration area. The unrecovered indent profile appears since the onset of plastic deformation and this is related to yield point. According to both von Mises and Tresca criteria, yielding takes place when the composition of stress, including the generating compressive stress plus the prior in-plane residual stress, reaches the criteria stress. Once the local residual stress is high enough (comparable to the material's normal yield strength) its effects on the yielding activation could not be overlooked. Apparently, the onset of plastic deformation will be promoted by tensile residual stress and inhibited by a compressive one, which in turn probably affects the final indent profile and thereby the modeling outcomes. On the contrary, the residual stress is very likely to be measured in PIP testing, which seems improbable in normal tensile testing and microhardness testing.

2.4.2 FSW sample effects

2.4.2.1 Sample anisotropy effect in FSW joint

Towards FSW materials, regardless of the inherent anisotropic microstructure of base material, many examples[32, 33, 34]have shown that the joint also shows anisotropic behavior in mechanical responses. This can be attributed to its non-homogeneous microstructure and texture evolved during the welding process while either material flow, temperature distribution, and strain diffusion is even. Figure 2.10 shows a good example of the microhardness measurement of an FSW joint sample (which is made of a titanium alloy), displayed in an anisotropic way. The measurements were carried out along two mutually perpendicular planes, as demonstrated in the left part. The first test line is made on the plane perpendicular to the rolled surface (TD-ND plane) whereas the second test line is basically located underneath and parallel to the rolled surface (TD-RD plane). Their corresponding hardness numbers show a similar trend but distinctive values over the different distances from the joint center. Hardness on TD-RD plane is overally greater than that on the TD-ND plane and the discrepancy is larger when the measured region locates much deeper from the joint center.

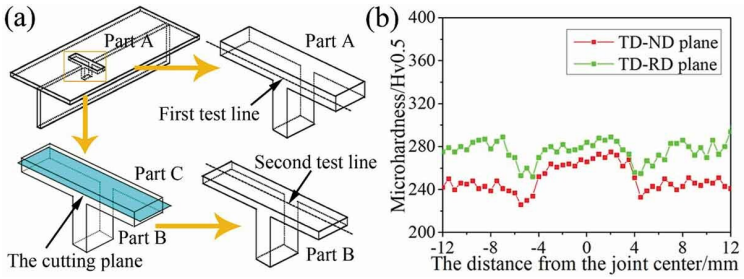

Figure 2.10: a) A Schematic illustration showing how the testing position is determined for microhardness measurement. b) a comparison of microhardness distribution in the two different cutting planes, taking the joint center as the base[33]

Figure2.11also shows a more comprehensive study of the anisotropic behavior of an FSW joint. The idea for its experimental design is to pick up the tensile specimens by cutting the joint plates at various angles. The basis of the anisotropy test is mainly established on a universal testing machine.

2.4.2.2 Residual stress effect in FSW joint

In a general way, metallic samples often contain residual stress and there commonly exists compressive residual stress in the subsurface of the sample when subjected to PIP testing. As a result, it makes the testing value of yield strength higher than its actual value, or i.e. material tends to appear slightly harder than it actually is under the indent. Apart from the general condition, some manufacturing processes also tend to introduce residual

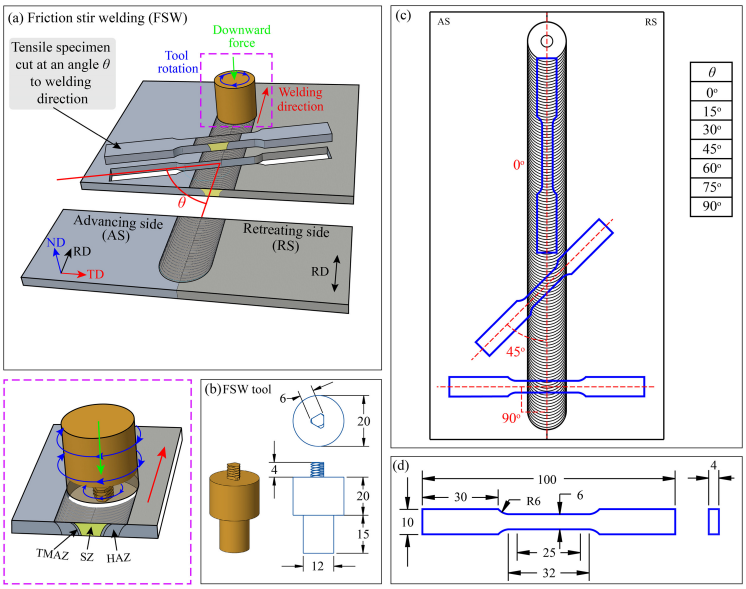

Figure 2.11: A schematic illustration of a) how the tensile specimen of the FSW joint is prepared for anisotropic measurement. b) dimensional information of the utilized FSW tool. c) various tensile specimens cut at different angles to the welding direction. d) dimension of the tensile specimen following ASTM standards. Note: all the dimensions are given in mm.[34]

stress inside the material sample. This also matters to the final testing outcomes of yield strength or stress-strain curve. When it refers to an FSW joint sample, residual stress also envolves over the welding region and demonstrates a unique distribution that varies with that emerged in other welding techniques. In the reported research of Y. Lim et. Cl[35], they measure the residual stress of an FSW steel joint (SUS409L) by the method of hole drilling towards different microstructural regions: thermo-mechanical affected zones in the retreating side and advancing side (TMAZ-RS, TMAZ-AS, respectively), stir zone (SZ), and base material region (BM). It was found that there was a considerable degree of compressive residual stress formed near the surface. When testing deep into 0.3 mm distance from the surface, a low level of tensile residual stresses emerge until the center of the SZ region. Whereas in the case of a tungsten inert gas(TIG) joint cut along the transverse direction(TD), it is tensile residual stresses that are formed in the fusion zone near the surface.

Broadly speaking, inhomogeneity refers to the spatial variations in the microstructure and properties of a sample. Since the indentation technique is only down to several hundred microns, picking up the variation between the near-surface region and the interior is of great importance. As has already been mentioned before, the presence of inhomogeneity can be derived from the surface preparation technique. Moreover, it is with certainty that the sample material may also exhibit inhomogeneity originating from manufacturing processes, such as the case-hardening treatment or a rolling process while the subsurface region undergoes higher plastic strain than in the bulk. In the above example, the studied

material also shows some level of inhomogeneity in residual stress distribution, which can be attributed to the FSW process. Unlike other regions that always present some low tensile residual stresses near the surface, SZ has some degree of compressive residual stress owing to the convex shape of the stir tool. In the welding region these differences in the formation of residual stress, as suggested, may make a difference in the mechanical properties of the joints. Meanwhile, they may also have potential effects on the acquiring process of indentation data.

2.4.3 Influence of sample preparation on indentation characterization

It is admirable that the overall requirement for sample preparation is fairly crude and simple when carrying out the PIP testing. That is to say, the finished sample surface could be accepted merely with a final treatment scale of a P2500 grit grind or finer. Furthermore, what is highlighted in the application of the indentation technique is its extended capability to identify some sample effects with relatively concrete information. From another perspective, those detailed sample effects, given by the PIP testing, can also be conducive to choosing/selecting some suitable models that would be applied in a particular area.

For example, if we define a target to find an optimized model which is going to be inserted into the inverse FEM method when the studied material is confined to an FSW steel joint. It would be inspiring to first think of how to prepare a sample for the right measurement aimed at providing sufficient judgments. To expand it, sample preparation issues can cover not only the surface technique but also the appropriate cutting plane, the right positions to be measured, the compared data while the sample effect is taken into account, and so on.

According to the discussion above, an FSW joint sample usually exhibits anisotropy characteristics on several planes (as shown in Figure2.11). Therefore this anisotropic response should be expected in one suitable model case. The testing planes can be therefore determined for acquiring such kind of information. From the experimental perspective, it looks much handier to make the testing samples in PIP testing only by creating several indentation planes as mentioned. Besides, residual stress in an FSW steel varies in different regions and the discrepancy is suggested significant. When utilizing an ideal model, the manifested outcomes of PIP testing are also expected to cover similar residual stress distribution. In the assessment of modeling, it is preferred to compare indentation data from some positions where residual stress difference is outstanding. From the given example, such a good option is to test from the surface to the center on the retreating side or to test at least a distance of 0.7 mm from the surface in different zones.

To sum up, it is worth discussing relevant sample effects issues when applying the indentation technique in one specified area. Based on the above discussion about anisotropy and local residual stress, some propositional guidelines for sample preparation are given.

When people carry out some experiments for modeling optimization, they could be helpful in further determining the indentation positions and what differences would be compared.

2.5 Highlighted theoretical background

2.5.1 Hertz model

When it regards a material's elastic property, one common way is to refer to the initial region of its stress-strain curve where the true stress proportionally increases with the true strain, and the ratio, given the name "Young's modulus", reveals this material's elasticity property. i.e. the capability of the material to reverse the deformation. The relation between stress/strain becomes a key topic when studying material's elastic behavior. In Hertz's contact theory[36], this concept is well illustrated by introducing a particular indentation stress and stress, defined as:

$$\sigma_{ind} = \frac{P}{\pi a^2} \tag{2.20}$$

$$\varepsilon_{ind} = \frac{4}{3\pi}\frac{h_t}{a} \tag{2.21}$$

For elastic part:

$$\sigma_{ind} = E_{ind}\varepsilon_{ind} \tag{2.22}$$

Those definitions originated from his analysis study on the stress distribution of the contact region between two contacted spheres. The contact radius, a, is defined as the radius of the projected area where two spheres come into contact with each other. It has been observed and analyzed that during the process of elastic contact, a is associated with the applied load P, the effective radius R_{eff}, and the effective elastic modulus E_{eff}, as expressed:

$$a^3 = \frac{3}{4}\frac{PR_{eff}}{E_{eff}} \tag{2.23}$$

According to the literature, he also inferred the relation between the contact radius a and the contact height "h_e" in the elastic component:

$$a = \sqrt{R_{eff}he} \tag{2.24}$$

The elastic contact model still demonstrates efficacy when applied to the spherical indentation case. This is achieved only by treating the flat material to be penetrated as a sphere with an infinitely large radius: $R_s = \infty$. See the schematic2.12 that depicts the special contact case. On this basis, he first defines the indentation stress that equals the mean contact pressure P_m and then refreshes the expression of the indentation stress when substituting into the analyzed equation of contact radius:

$$P_m = \frac{P}{\pi a^2} = \{\frac{4}{3}\frac{E_{eff}}{\pi}\}\frac{a}{R_{eff}} \tag{2.25}$$

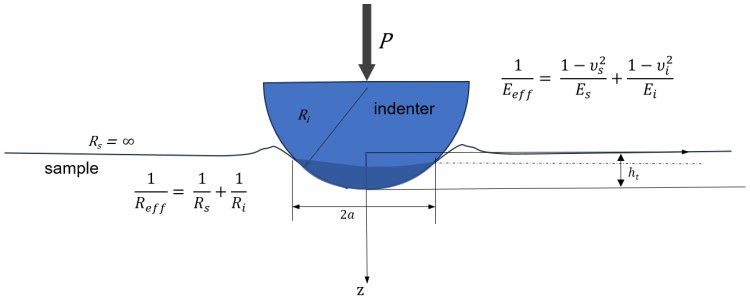

Figure 2.12: The spherical indentation case when relating with Hertz contact model

In analogy to the stress-strain relation within the elastic region from the true stress/strain curve, the expression of the defined indentation stress gives a new interpretation of indentation strain, which is:

$$\varepsilon_{ind} = \frac{a}{R_{eff}} \frac{3}{4} \pi \tag{2.26}$$

The indentation stress-strain relation in the elastic part is also analogous to the common sense that they are proportional with a constant, named effective elastic modulus. Since there are two main bodies involved in the contact procedure, the indentation modulus is considered to carry both of their elastic information. The analyzed expression is shown as:

$$\frac{1}{E_{eff}} = \frac{1-\mu^2}{E_s} + \frac{1-\mu_i^2}{E_i} \tag{2.27}$$

Where the subscripts "i" and "s" refer to the indenter and the sampled material.

In addition to the definition of indentation stress and strain, another valuable aspect is the provided theoretical relationship between the load P and the elastic penetration depth h_e, as given below. This is obtained by simply substituting the equation 2.23 into the expression for the mean contact pressure (equation 2.25). The resulting relation expression is considered to hold significant practical value for further analysis of indentation data, and this will be addressed in the following experiment part of the thesis.

$$P = \frac{4}{3} E_{eff} R_{eff}^{\frac{1}{2}} h_e^{\frac{3}{2}} \tag{2.28}$$

2.5.2 Determination of contact radius

During indentation, the contact area/radius consistently changes, and it is unrealistic to pick up all the instantaneous contact radii. According to the literature, it is preferred to capture the contact radius at or close to the peak indentation load since a great number of models were reported under this circumstance. When the contact radius model is applied to one specific scenario, it also requires careful recognition of which contact radius model is the most suitable for the applied indentation system, including but not limited to the sampled

material, the indenter size and geometry, and the maximum indentation depth. Below are three candidate models that are supposed to be well applied in the thesis.

In the above subsection, the Hertz contact theory has proposed a relation expression to describe a frictionless contact procedure between two linear isotropic elastic materials with quadratic surfaces, as "$a = \sqrt{R_{eff} h_e}$". However, this contact radius estimate heavily relies on the elastic depth capture, which is challenging to be achieved in the practical measurement.

The second introduced model adopts the initial unloading stiffness S and the effective modulus to estimate the contact radius at the peak load (the starting point of unloading). While it also takes account into the indenter geometry using the factor β.

$$a = \beta \frac{S}{2E_{eff}} \tag{2.29}$$

The third one is from the Oliver-Pharr model, as introduced in this chapter already (see "Indentation data conversion - In semi-analytical" section), the contact radius and the contact depth follow the derived expression as:

$$a = \sqrt{2h_c R_i - (h_c)^2} \tag{2.30}$$

Here the contact height "h_c" is estimated by the total indentation depth and the corresponding peak load, both of which can be experimentally measured, through the expression:

$$h_c = h_t - \beta \frac{P}{S} \tag{2.31}$$

Where the β donates the geometrical factor of the indenter, and the S refers to the unloading stiffness. Detailed information is provided in the section "Indentation data conversion - In semi-analytical".

2.6 Conclusion and research objectives

2.6.1 Concluion and research gaps

In this literature review, the indentation-based local characterization has been well elaborated through several aspects, ranging from the raw indentation data capture, the indentation data conversion into the equivalent stress-strain curve, as well as a specific application case study in friction stir welding steel. Relevant fundamentals and some underlying features of this novel method have since been elucidated. Based on the literature study, two prominent aspects involved in the methodologies of indentation data conversion have been discussed in detail. The following makes a summary and delineates the research gaps associated with each of them.

1) The semi-analytical method primarily relies on load-displacement data and the data conversion is based on the specific contact model solution that combines both analytical and numerical techniques. It performs well in capturing the material's Young's modulus and yield strength under the stated material-indenter contact system. **There is a lack of comprehensive studies in revealing sample's complete plasticity behavior using this approach or trying to figure out the reason behind it; Practical research also faces challenges with model compatibility when applying a well-stated semi-analytical model to a new contact system.**

2) Similar to the instrument load-displacement data, indentation data of residual profile also widely serves in the IFEM method and enables to inferring more concrete plasticity parameters of the sampled material. However, the indentation data focuses on the permanent deformation of the indented material and hardly indicates any elastic information through the working principle of the IFEM. In analyzing the entire indentation process, it is observed that the material's contact surface always reproduces the indenter's bottom shape during loading. Upon unloading, the testing material surface takes the elastic recovers from its original deformed state to what it is like in the residual indent profile. It suggests that the initial and final states of the material's elastic deformation can be determined and one of them could be analyzed through the residual indent profile data. **However, there is a lack of feasible study in capturing the elastic property by the extra data support of the residual indent profile.**

2.6.2 Research objectives

The following research objectives are formulated based on the research gaps addressed in the literature study:

1. Assess the compatibility between a provided semi-analytical model and a specific material to acquire its local properties of Young's modulus and yield strength. Specifically, to investigate the model's compatibility issue, the following aspects need to be addressed:

a. the choice of indenter
b. the determination of load parameter
c. determination of load-unload cycles

2. Develop a method that extracts material's Young's modulus from its unloading/reloading responses. To accomplish this objective, two major research questions are involved in this topic:

a. how to establish the analytical model based on material's mechanical responses in unloading and reloading ?
b. how to design practical experiments to validate the model? (specific study aspects can refer to the above.)

Chapter 3

Semi-analytical model validation

An established semi-analytical model was introduced to extract Young's modulus and yield strength of DH36 steel material locally. It was ascertained performed well with the hardware measurement system at the Georgia Institute of Technology. We aim to set up practical experiments to investigate its applicability with the testing system in-house. Several practical measuring issues are expected to arise when the model is applied to a new contact system, such as the choice of indenter, the setting of load, the determination of the number of load-unload cycles, etc. Related details will be addressed in the section "Experiment setup". As for the semi-analytical model itself, the indentation strain and indentation stress, both related to the contact radius, are highlighted for constructing a representative strain-stress curve. Specific information about the establishment of the semi-analytical model will be elaborated in the subsection of "Data processing". Relevant results and discussions about the resulting indentation strain-stress curves, elastic modulus estimates, and yield strength estimates will be presented separately in this chapter.

3.1 Data processing

3.1.1 Indentation strain/stress

In this semi-analytical model, indentation strain and indentation stress follow the formulation proposed by Kalidindi and Pathak[37], as shown in equations3.13.23.3. According to the reported article, this indentation strain model was confirmed reliable by the means of Finite Element predictions when it was applied to the elastic-plastic contact between the diamond-like indenter and sampled material of Aluminum or Tungsten. However, there remains uncertainty regarding the adaptability of the indentation strain/stress model to our investigated contact system.

$$\sigma_{ind} = \frac{P}{\pi a^2} \tag{3.1}$$

$$\varepsilon_{ind} = \frac{4}{3\pi}\frac{h_t}{a} \approx \frac{h_t}{2.4a} \tag{3.2}$$

For elastic part:

$$\sigma_{ind} = E_{eff}\varepsilon_{ind} \tag{3.3}$$

In these given expressions, of particular note is the indentation strain ε_{ind}. Inspired by Hertz's contact model, the elastic height h_e in the original elastic indentation strain "$\varepsilon_{ind} \approx \frac{h_e}{2.4a}$ " is substituted for the total depth h_t to unify the expression of indentation strain both in pure elastic indentation and elastic-plastic indentation. This allows the h_t to be directly measurable as the load P. Meanwhile, the defined indentation strain also provides a specific physical meaning, which is in some way analogous to the physical meanings of a normal strain demonstrated in one compressing procedure: an original cylindrical object of radius a and height $2.4a$ is compressed to a cylinder with the height of h_t while ignoring the radial change. It indicates that any single indentation procedure has an idealized primary zone of which size is based on the contact area, and the indentation strain "$\varepsilon_{ind} \approx \frac{h_t}{2.4a}$ " is defined as the ratio of actual deformation to the idealized one.

In the above equations, the left parameter of contact radius a is determined through the improved Oliver-Pharr model[23], which is supposed to be well applied to the shallow indentation case, expressed as below.

$$a = \sqrt{2h_cR_i - (h_c)^2} \tag{3.4}$$

$$h_c = h_t - \beta\frac{P}{S} \tag{3.5}$$

Another two contact radius models: the Hertz model for quadratic surface[36] and the relative stiffness model[23], are also utilized for results comparison. The latter relative stiffness model, which also appeared in the analysis work of Oliver and Pharr, can be applied to any indenter geometry characterized as a smooth function body of revolution. Relevant information about the three models is provided in the section "Highlighted theoretical background" in Chapter 2. Besides, it should be noted that the calculated contact radius a is always at or close to the peak indentation load and has to rely on each unloading segment in the P-h curve. Therefore, the amount of the unloading segments contributes the same amount of the indentation strain/stress point.

After determining all the parameters involved in the expressions of σ_{ind} and ε_{ind}, the representative indentation stress-strain curve is preliminarily established. However, it should be noted that the original point collected by the practical instrument depends on a threshold change of detected stiffness. Influence factors such as the oxide layer, contaminants upon the material surface, or even the surface roughness tend to make the instrument-detected zero-point for indentation not fit in what is described in the semi-analytical model. For instance, indentation-depth-dependent parameters, such as the contact radius, may not be

reasonably solved, thereby generating incredible σ_{ind} and ε_{ind} for the construction of indentation strain-stress curve.

To determine the effective zero-point, we iteratively take several datasets in the initial loading segment and seek an ideal data scope that best fits with Hertz's elastic contact model, through the equation:

$$P - P^* = \frac{4}{3} E_{eff} R_{eff}^{\frac{1}{2}} (h - h^*)^{\frac{3}{2}} \tag{3.6}$$

The starting point of the target datasets is treated as the effective zero-point (P^*, h^*). In this context, the indentation stress and strain turn to "$\varepsilon_{ind} \approx \frac{h_t - h^*}{2.4a}$" and "$\sigma_{ind} = \frac{P - P^*}{\pi a^2}$", respectively, producing a more reasonable indentation strain-strain curve.

3.1.2 Extraction of effective modulus

The extraction of the indentation modulus (or the effective modulus) refers to both the fitting result from the effective zero-point determining and the slope of the initial proportional part from the indentation stress-strain curve. Specifically, We first estimate the effective modulus through the former way in which the modulus is solved when the best fit of the first initial pure elastic region has been found. This solved effective modulus leads to the contact radius estimate either from the Hertz model or the relative stiffness model. After establishing the indentation strain-stress curve, the second approach is employed to settle the slope of the pure elastic segments in the $\sigma_{ind} - \varepsilon_{ind}$ curve as the other effective modulus estimate. The two E_{eff} estimates are further taken comparison.

3.1.3 Extraction of yield strength

Compared to the conventional uniaxial tensile test, the strain caused by indentation is not distributed equally along the indentation axis within the material and so is the radial distribution in strain. Therefore it is hard to identify the yield point for the indentation-based test because the yield takes place in some material regions but is usually along with some unspecified materials undertaking the elastic deformation. Due to the fact that the contact stiffness $\frac{dP}{dh}$ varies in elastic response and plastic response, we singled out the unspecified elastic deformation before yield in a range of 0.95 to 1.3 times of elastic stiffness estimate. The analytical elastoplastic part was thus confined to the region where the stiffness is considered higher than 1.3 times of elastic stiffness estimate.

In this thesis, a new definition of yield strength has been proposed that takes the plastic offset percentage to account for the elastic-plastic transition zone. The yield point is confined to the beginning of the elastoplastic region in the corresponding $\sigma_{ind} - \varepsilon_{ind}$ curve, in which case the plastic strain equals 25% of its elastic strain. "25%" is the plastic offset percentage and is altered in different elastic-plastic transition behavior of the testing material.

3.2 Experiment setup

For the semi-analytical model, its corresponding practical experiments are based on the cyclic indentation tests. A spherical Tungsten-Carbide indenter with a radius of 14 mm was adopted. Young's modulus of the indenter material is about 600 GPa. The instrument data of load and displacement from 15 cycles of load-unload indentation procedure was collected through the ZwickRoell Z2.5 hardness tester. Specific settings of loading parameters are illustrated in the schematic 3.1, where an extra depth of 0.4 μm was added after one cycle. The deformation rate was set as 0.1 mm/min for the loading procedure whereas it was set as 6 mm/min for the unloading part.

Parameters	Value or remark
Number of cycles	15
Point of load application (standard force)	5 N
Increase per cycle: indentation depth	0.4 µm
Speed load application	0.1mm/min
Hold time between adjacent cycles	5s
Hold time at the point of load removal	5 s
Types of hold during waiting time	Force controlled
Point of load removal (standard force)	2.5N
Load remove speed	6 mm/min

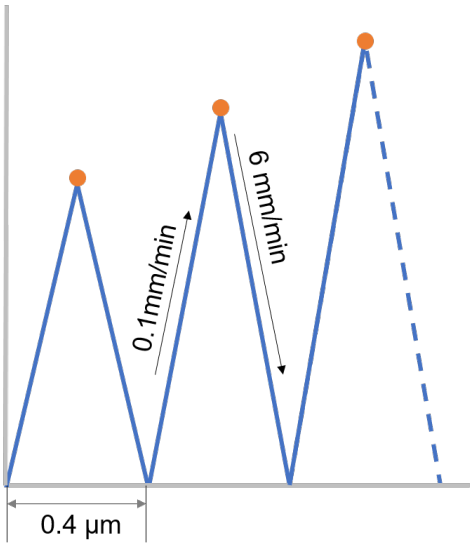

Figure 3.1: Loading parameters of the cyclic indentation tests on Zwick hardness tester

3.2.1 Loading parameters setting

To create a suitable program for the spherical indentation tests, what deserves the most attention might be the loading setting. According to the "Experiment setup", there were 15 cycles of load-unload, contributing enough stress/strain points for a reliable construction of the $\sigma_{ind} - \varepsilon_{ind}$ curve. The maximum load or penetration depth during the entire indentation process is required to produce a measurable indentation without causing excessive deformation or damage to the testing material. By referring to the literature, the target indentation depth is less dependent on the size of the spherical indenter or the loading system, making it much easier to identify compared to the maximum load. We assume the same level of penetration depth as the peer work. The maximum depth was fixed at approximately 6 mm,

with an equal allocation of 0.4 mm in each cycle. The deformation rate is mainly specified in accordance with the category of the testing material. For ductile metals, the loading rate is usually set as 100 μm/min for adequately capturing material's indentation responses, and the unloading rate was generally 100 μm/s as suggested by peer work.

3.2.2 Chioces of indenter and sampled material

As for the indenter used in the experiments, its spherical geometry ensures a consistent spherical shape of the contact area regardless of the penetration depth. This so-called self-similarity characteristic enables the mathematic model, which relates the contact area (or radius) and the indentation depth, to be well applied in both the elastic part and plastic part. Besides, compared to some sharp indenters such as the Vickers and conical indenters, the spherical indenter causes a smoother stress field within the material, allowing a better capture of the evolution with respect to material's indentation responses[37]. The choice of the indenter radius was taken at 14 mm, and this is aimed to evaluate whether a relatively shallow indentation case can be applied with the semi-analytical model. Besides, compared to the smaller indenter tip case under the same loading setting (i.e. causing the same penetration depth at each cycle), the larger spherical indenter case allows for sharper peaks or valleys in the plot of displacement which is more propitious to distinguish different unloading/loading stages.

A common base material stainless steel DH36 for the friction stir welding is adopted as the main study material for the validation process. In terms of one of the promising application fields in FSW joint property research, primarily taking the parent material as the experimental material of interest makes a great difference. This is due to several reasons, as shown below:

1. In general, the process of friction stir welding tends to produce weld joints with properties that are similar or sometimes superior to those of the base materials. The corresponding property values and their mechanical responses to external stress are usually around the same level.

2. From the perspective of the characterization technique, it should be noted that the property results are only dependent on its response toward the applied stress, rather than the type of material. Taking the parent material as the studied subject does not affect the application of other types of material such as FSW joint material.

3. In addition, it is easier to make a reference object when validating a novel characterization method using a homogeneous base material rather than a joint material. On the one hand, there is hardly any doubt about gaining an accredited local property of a homogeneous material through the conventional uniaxial method (i.e. the local property is supposed to be well represented by the bulk property in this case). On the other hand, the selected base

material is more easily controlled to meet homogeneity compared to the welding joint.

Besides, it is worth mentioning that the testing material of steel DH36 may manifest anisotropic features in both elastic and plastic properties, and this is inherently due to its manufacturing rolling process in reality that the resulting properties may fairly vary in the loading directions. Nevertheless, in the validation design for local characterization, such features inspire us to extend the comparison dimension within one participant sample by analyzing its anisotropic mechanical behavior under different test systems.

3.2.3 Sample preparation

The main purpose for sample preparation in indentation tests is that some sample-related factors, such as the inherent surface roughness, the effects of contamination, and oxide film, tend to affect the initial point of contact with the indenter and thus cause data noise at the beginning. Hence, a series of standard metallography processes were carried out on the given DH36 samples to ensure a smooth and flat region for testing. Specifically, this is done by successive grinding steps using the silicon carbide papers in the range of 180 - 320 - 1200 - 2000 grit, followed by two chemical polishing steps using 3 μm and 1 μm diamond suspension.

3.3 Results

3.3.1 Indentation stress/strain curve

The experimental load-depth (P-h) curve directly output by the Zwick machine is shown in Figure3.2. When it comes to converting to the indentation strain-stress curve, we have adopted three different contact radius models for figuring out the representative points of σ_{ind} and ε_{ind}, respectively. The three contact radius models are demonstrated in table3.1

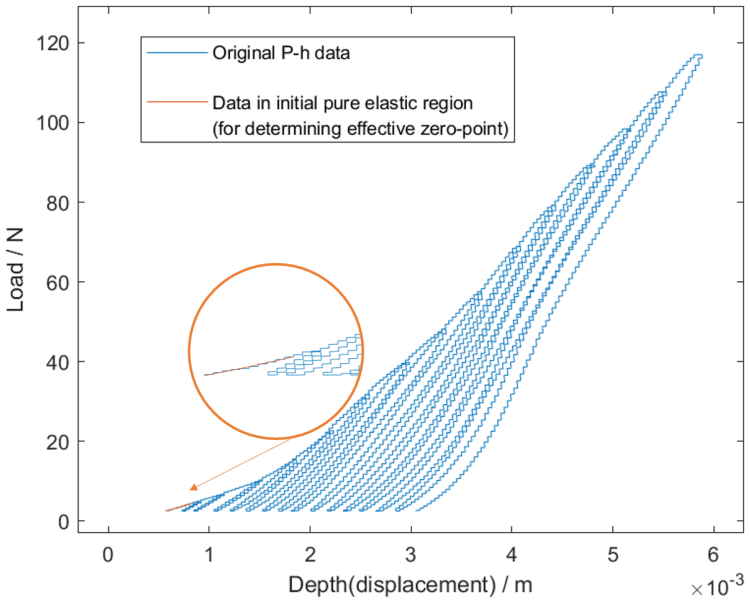

Figure 3.2: The experimental load-depth curve for the introduced cyclic indention tests. Some of the initial data in orange represents the used datasets for determining the effective ”zero-point”.

Table 3.1: Three contact radius models with mathematic expressions

Contact radius model	Expression
Oliver-Pharr model	$a = \sqrt{2h_cR_i - (h_c)^2}\ h_c = h_t - \beta\frac{P}{S}$
Hertz model	$a = \sqrt{R_{eff}h_e}$
Relative stiffness model	$a = \frac{S}{2E_{eff}}$

Their corresponding indentation stress/strain curves are presented below. Thereinto, the yellow line represents the fitting result of the elastic part estimate. The orange line shows the rearrangement of the defined strain offset curve, encompassing all cases where the elastic strain and plastic stain satisfy the relation of $\varepsilon_p = 0.25\varepsilon_e$. The purple line indicates the estimate of the indentation strain/stress point at the initial elastoplastic region.

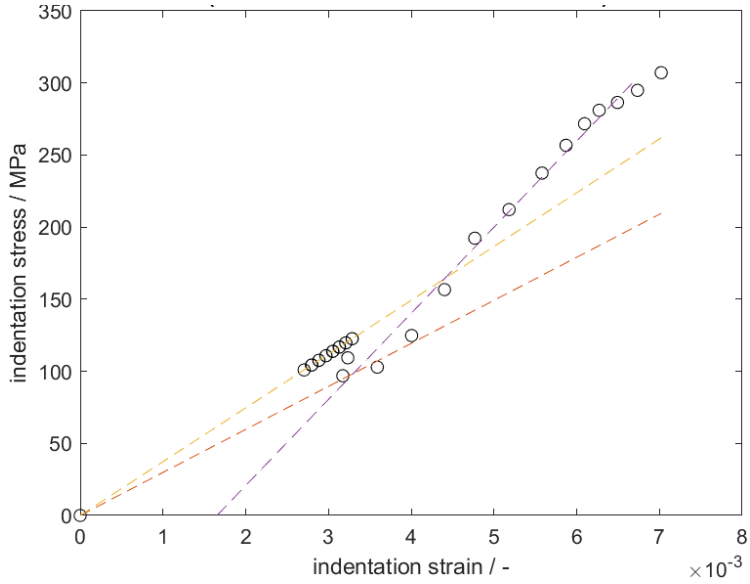

Figure 3.3: The indentation strain-indentation stress curve output using the Oliver-Pharr contact radius model. Yellow line: elastic part estimate. Orange line: modified strain offset curve. Purple line: estimate of initial elastoplastic region.

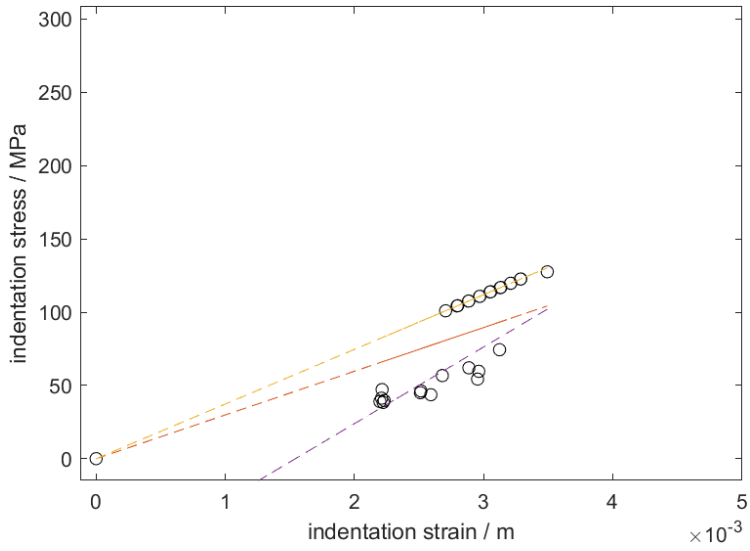

Figure 3.4: The indentation strain-indentation stress curve output using the Hertz contact radius model assuming a quadratic surface. Yellow line: elastic part estimate. Orange line: modified strain offset curve. Purple line: estimate of initial elastoplastic region.

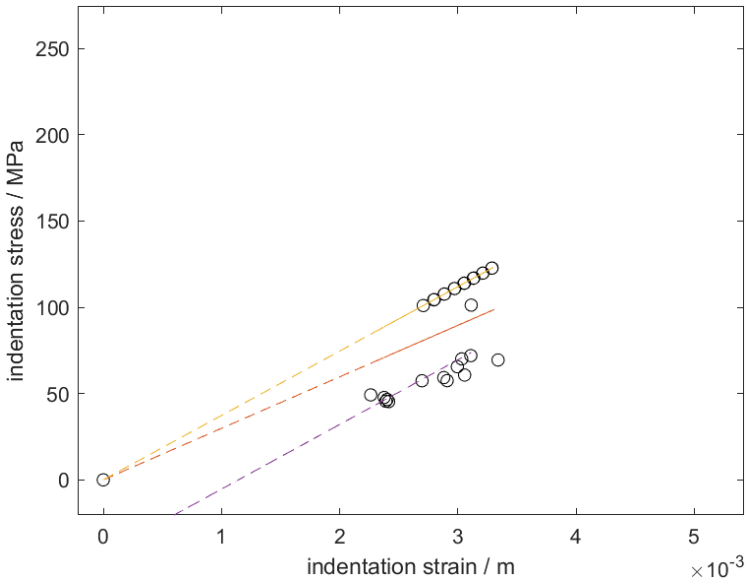

Figure 3.5: The indentation strain-indentation stress curve output using the relative stiffness contact radius model. Yellow line: elastic part estimate. Orange line: modified strain offset curve. Purple line: estimate of initial elastoplastic region.

3.3.2 Effective modulus estimates

The corresponding effective modulus estimates are listed in the table3.2. we have mentioned two different methods to solve the effective modulus, one is from the Hertz model fitting when determining the effective zero-point (E_{eff} estimate 1). The other refers to the slope of the final obtained indentation strain-stress curve (E_{eff} estimate 2), which might be varied in the chosen contact radius model. As shown from the results, both of the E_{eff} estimates have reached a considerable consensus.

Table 3.2: Results of effective modulus estimates

Contact radius model	E_{eff} **estimate 1**	E_{eff} **estimate 2**
Oliver-Pharr model	37.318 GPa	37.303 GPa
Hertz model	37.318 GPa	37.303 GPa
Relative stiffness model	37.318 GPa	37.318 GPa

3.3.3 Yield strength estimate

From the representative indentation strain-stress curve in all three cases, it is impossible to figure out the yield strength estimate using the strain offset curve since the functional curve (the orange one in the $\sigma_{ind} - \varepsilon_{ind}$ curve) could not link to any point in the elastoplastic

region. The function curve passed through the origin point and did not look the same as the well-defined strain offset curve that was supposed to parallel the yellow curve with a slope of indentation modulus (effective modulus). But in fact, it was deduced from the strain offset curve that contains all $\sigma_{ind}/\varepsilon_{ind}$ points in accordance with the ideal condition of $\varepsilon_{p,ind}$ = $0.25\varepsilon_{e,ind}$, where 0.25 regards the percentage of strain offset we have set.

3.4 Discussion

3.4.1 The abnormal indentation strain-stress curve

In all three $\sigma_{ind} - \varepsilon_{ind}$ curves, obviously, the stiffness of $\frac{d\sigma_{ind}}{d\varepsilon_{ind}}$ in the "defined" elastoplastic region is higher than the stated elastic region unexpectedly. Therefore, it would never figure out our defined yield strength point that is supposed to intersect with the strain offset line above the elastic part. This is super abnormal for structural steel material as strain hardening almost always occurs after the yield point and the stiffness of $\frac{d\sigma_{ind}}{d\varepsilon_{ind}}$ is at least lower than that in the elastic part.

3.4.2 The abnormal effective modulus estimate

The estimate of effective modulus is considered precisely captured from the two close estimates (37.303 GPa vs 37.318 GPa) through two different ways: one is from the direct result of Hertz equation fitting when determining effective "zero-point", and the other is obtained from the proportional part of the $\sigma_{ind} - \varepsilon_{ind}$ curve at the beginning. However, the estimated value, which is about 37 GPa, is not valid as the indentation modulus is expected to be around 310 GPa, which is almost ten times larger than the experimental result. (The expected modulus of 310 GPa refers to the effective modulus expression present in Figure2.12 with the indenter modulus of 600 GPa and the sampled material's tensile modulus of 204 GPa).

3.4.3 Comparison with the example results

For comparison, an experiment data of the P-h curve provided by the Georgia Institute of Technology is presented below in Figure3.6. Its relevant measuring issues such as sample preparation, and measurement parameters settings are almost comparable to our case but the example case utilizes the testing machine of Zwick/Roell Z100 with a 6.35mm-radius indenter. Apparently, there is a significant difference between the two P-h curves in the initial datasets which is used for estimating the effective zero-point. When importing the data into the same processing program using the Oliver-Pharr contact radius model, the obtained effective modulus is 169 GPa with an approximate sample's Young's modulus of 209 GPa. Indentation yield strength and yield strength estimates are 784 MPa and 392 Mpa, respectively. Those are considered reliable results when compared to the similar values of tensile results from the same homogeneous material: Young's modulus is 204$\pm$7 GPa, and yield

strength is 391±0 MPa.

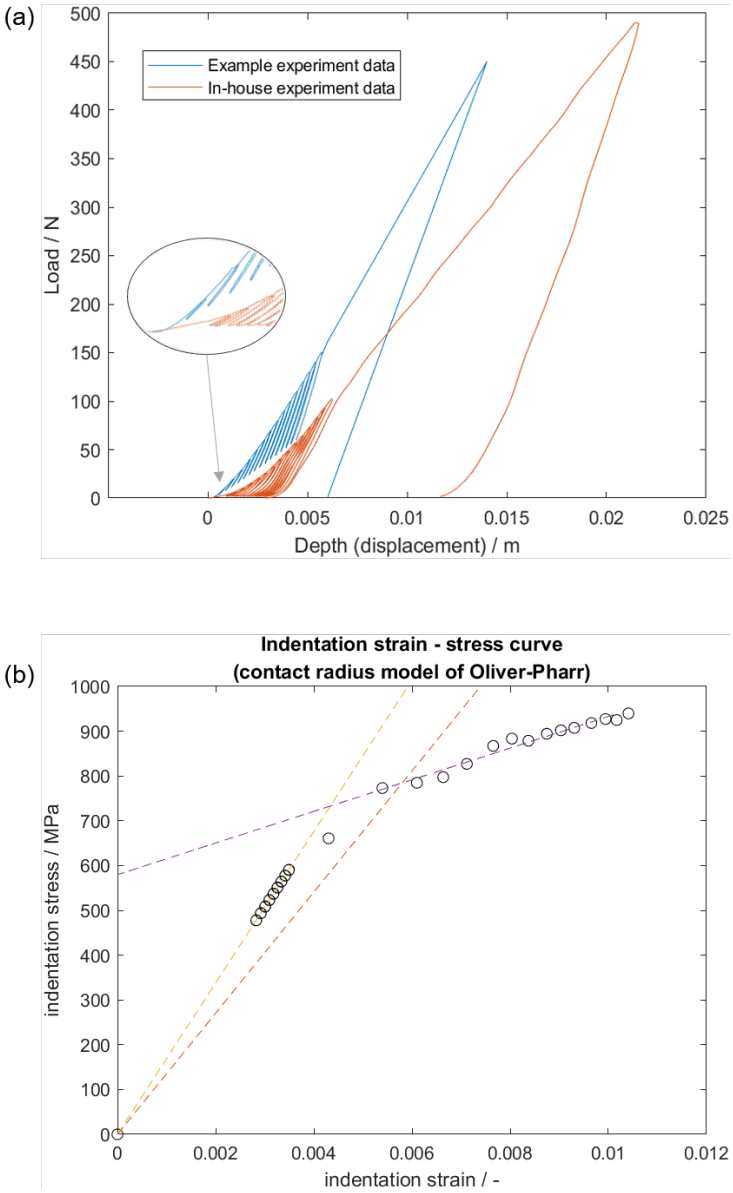

Figure 3.6: a. Comparison between the two experiment data. b.The indentation strain-indentation stress curve generated from the experiment data provided by Georgia Tech, using the Oliver-Pharr contact radius model. Yellow line: elastic part estimate. Orange line: modified strain offset curve. Purple line: estimate of initial elastoplastic region.

Hence, it can be concluded that the data output by the Zwick machine in our lab appears unrealistic according to the analysis above. The main reason may be owing to the load-sensing system that did not capture the first point when contacting the sample solid. From the converted $\sigma_{ind} - \varepsilon_{ind}$ curve, those representative $\frac{\sigma_{ind}}{\varepsilon_{ind}}$ curve points are prone to be located in the region after elastic-completely region or the post-yield region. This is because it is possible and quite common that the constant stiffness $\frac{d\sigma_{ind}}{d\varepsilon_{ind}}$ at the beginning is lower than that of the latter proportion. In this context, it indicates the collection of indentation data is more likely to be started from relatively deep penetration, rather than starting at the beginning of the indentation.

From the other perspective, the experimental results also point out our semi-analytical model has a great dependency on the hardware instrument and load step setting, particularly in the determination part of effective zero-point. Usually, the testing system, such as the Zwick machine in our case, has its own "zero-point" correction and is thought to eliminate or adjust the initial data signals by its default procedure[38]. In this context, some raw indentation data that covers the pure elastic responses or even the yield behavior of the direct-contact material (represented by stages I and II, as shown in Figure3.7) is likely to be missing. This is probably caused by the wrong zero-point identification within the machine itself.

While the reduced output data, however, is more likely to merely reveal the properties of local material in the indirectly affected zone. This indirectly affected material zone, as illustrated in the blue region of stage-III in Figure3.7, tends to alter its material scope of influence with the increasing depth of penetration, making it much harder to capture an entire indentation response when compared to one constant material zone with an equal strain allover. One of the solutions is to apply different loads in a staged way, such as the cyclic indentation tests here. It is inherently to capture as many mechanical responses as possible of firstly the direct contact material and secondly the indirectly affected material under different peak loads. In our semi-analytical model, some solved parameters, such as E_{eff}, are processed ideally based on the direct contact material and play important roles in further data processing that reflects the behavior of indirectly affected material. Thus a good application of the model requires a very matched design of "zero-point" identification in the indentation testing machine.

Furthermore, even with a good indentation testing system with a tolerable "zero-point" correction, it also raises a challenge on how to determine the amounts of the load cycle and the load steps between each cycle that just precisely capture the exact pure elastic responses of the direct contact material, as well as the initial point where plastic deformation begins.

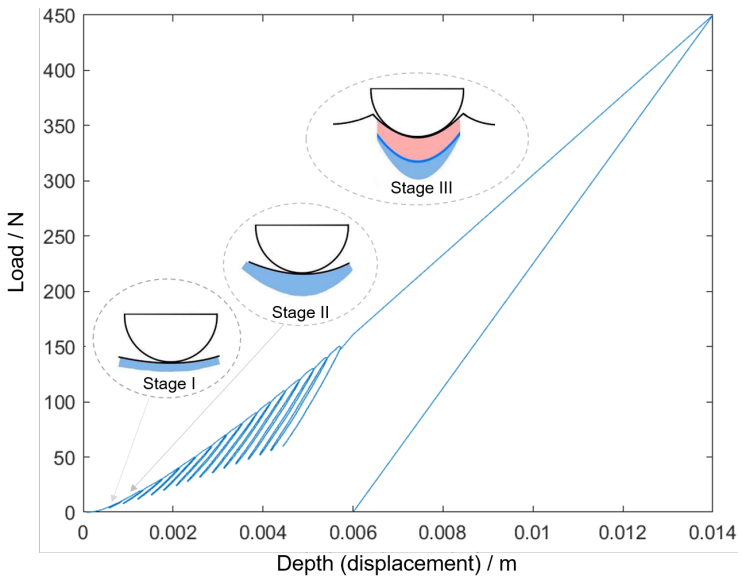

Figure 3.7: Schematic depicting the behavior of the testing material surface during cyclic indentation tests. First, to concern the single indentation procedure, the behavior of the testing material can be divided into 3 stages: Stage I represents the initial elastic contact with the indenter, where the material underneath the indenter in the blue zone undergoes elastic deformation. As the applied load increases, the elastic deformation zone expands (Stage II). Plastic deformation initially occurs in the most stressed material zone which is directly underneath the indenter (shown in pink), while the further indirectly contacted material zone still undergoes elastic deformation (shown in blue) and continues to expand. With further load increase, both the elastoplastic and elastic regions continue to expand along the indentation depth. The cyclic indentation aims to decompose the single indentation test, allowing stages I, II, and III to be separately captured across multiple cycles.

Chapter 4

Extraction of effective modulus by additional profilometry

In the Chapter of "semi-analytical model", the extraction of effective modulus relies on the fitting program concerning the Hertz elastic contact model 2.28 and the clarified elastic data during the initial contact. This also leads to the determination of the so-called effective zero-point by defining it as the first point of the best-fit datasets that primely conform to the Hertz equation. However, when it comes to practical applications, this approach imposes high demands on the hardware indentation testing system. It requires the testing system not only to minimize data noise as much as possible, but also to enable a reliable "zero-point" correction so that the recorded initial data still covers the pure elastic responses of the testing material. This is quite difficult to achieve based on the current indentation testing system in-house.

In this context, another scheme for effective modulus capture is developed and its overview is well summarized in Figure4.1. From the scheme overview, in addition to the instrument data of load-displacement during indentation, another type of indentation date, residual indent profile, was conjointly employed. This research aims to develop a novel method for extracting the effective modulus of the indenter-sample contact system with the assistance of profilometry. This chapter begins with the establishment of the novel method and elaborates it through two research questions:

1. how to establish the analytical model based on the two indentation data? (Section of "The analytical model establishment")

2. how to design practical experiments to validate the model? (Sections of "Data processing" and "Experiment setup")

Detailed information for the two indentation data processing will be specifically demonstrated in the section of "Data processing". Relevant results and discussions will be presented separately in this chapter.

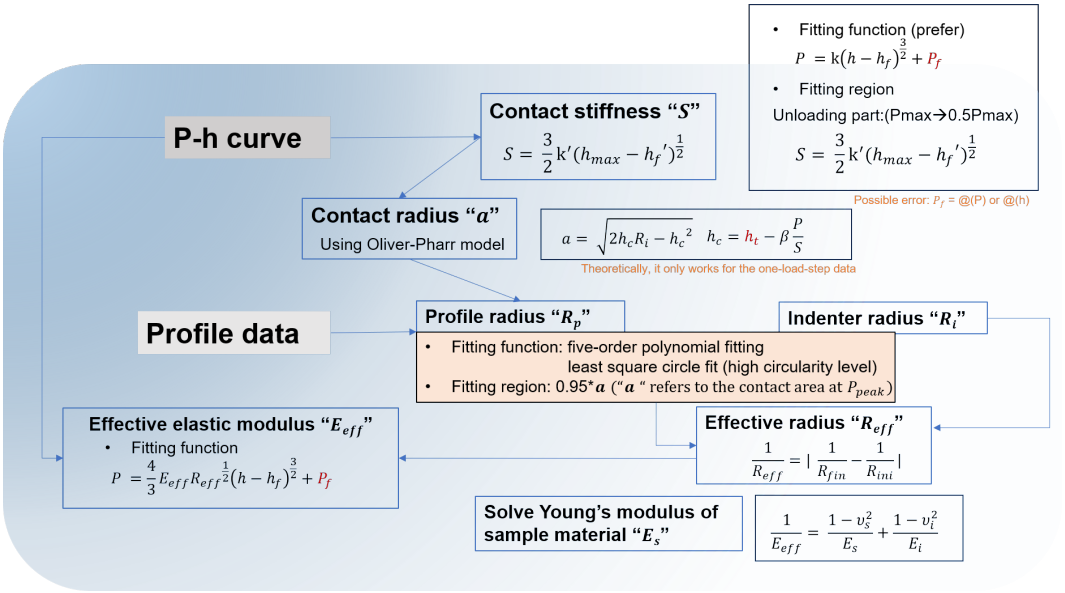

Figure 4.1: Overview of the elasticity extraction through the Hertz model fitting program

4.1 The analytical model establishment

Similar to the "semi-analytical model", the novel method also determines the effective modulus through fitting with the same Hertz equation2.28. However, a key difference lies in the data region used for fitting. Instead of the elastic data defined at the initial, the method utilizes the unloading or reloading segments as the fitting regions, both of which demonstrate an extensive data size compared to the former case. The unloading segment was regarded as elastic because when subsequent reloading is applied at the beginning, it often reproduces the unloading part of the load-depth curve at the same spot, indicating that the changes in displacement are almost reversible with the applied load. Thus, the two data segments both from unloading and reloading are considered suitable fitting candidates, though it raises a concern of which region works best when fitting with the Hertz equation.

When fitting the unloading segments to the Hertz contact model, it necessitates the determination of effect radius "R_{eff}". Originally in Hertz contact theory, R_{eff} refers to the curvature radius of the contact area between two contacting bodies and is also used to characterize the stress distribution within the material. But when it comes to the specific Hertz equation of interest, the effective radius is usually simplified to only involve the sample radius and indenter radius, making it look more based on the geometric consideration. However, such a simplification of R_{eff} might be practical when applied in the initial contact procedure of the spherical indentation but may not fully capture the intricacies of the contact mechanics or stress distribution for the elastic unloading procedure, where the deformed material relieves the residual stress to push the indenter up in a controlled way. Here, we assume R_{eff} in the Hertz equation tends to more likely represent the changes of

the deformed surface, as described below:

$$\frac{1}{R_{eff}} = \left| \frac{1}{R_{fin}} - \frac{1}{R_{ini}} \right| \tag{4.1}$$

Where R_{ini} and R_{fin} refer to the initial and final curvature radii at the bottom of the testing surface of the sampled material along the indentation axis, respectively. When it regards the case of the elastic unloading procedure, the initial deformed state always follows the spherical indenter bottom (donated by R_i)while the final deformed state could be characterized by the profilometer in principle (donated by R_p). This procedure can be well illustrated in the schematic 4.2

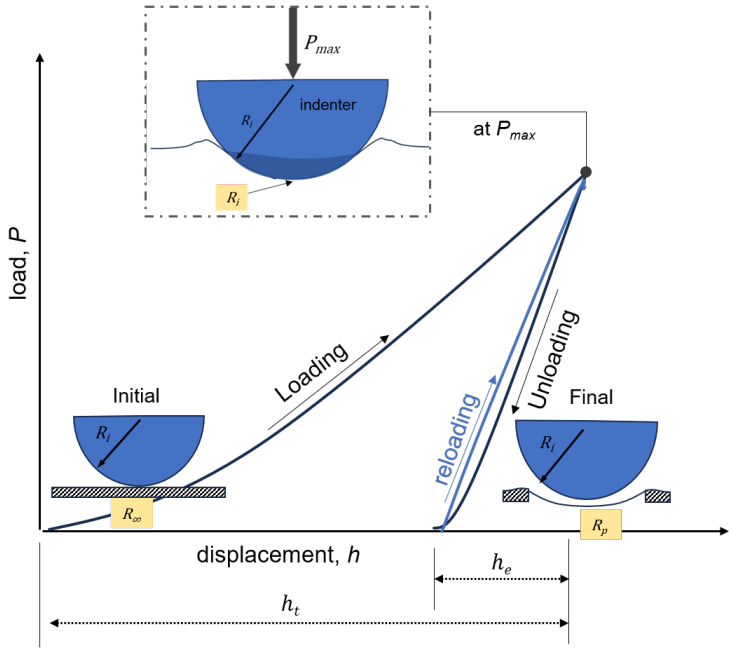

Figure 4.2: A single load-unload indentation tests with stage demonstrations in the indenter-sample contact region

It is worth noting that this effective radius interpretation could also be well applied in the original simplification of R_{eff} that both of them donate the same values. Take the loading procedure as an example. The initial sample surface state could be considered perfectly flat whereas the final surface state of the contact material always replicates the shape of the harder indenter bottom, causing the R_{ini} and R_{fin} to take the values of ∞ and R_i, respectively. The R_{eff} equals the indenter radius R_i, which is in accordance with the calculated results R_i from the original R_{eff} definition (R_s is also treated as ∞). The same conclusion could also be drawn from the reloading procedure where the initial surface state of the testing region is curved. The curvature radius of the deformed surface before contactting donates the R_{ini} while the indenter radius R_i regards the final state of the reloaded sample surface R_{fin}. Whereas from the original definition, R_{eff} involved a negative value of R_s, which

refers to the negative curvature radius of the deformed surface, along with a positive value of R_i. The resulting effective radius has the same expression and value as that from the new perspective.

Hence, we suppose it feasible that R_{eff} in the Hertz equation characterizes the change of the contact area between the initial and final state. Since the sampled material is the most deformable entity, we take its contact surface as the main study subject. When linking to the actual condition, the analyzed "R_{ini}" or "R_{fin}" is either equivalent to the indenter radius or associated with the final indent profile after unloading. For ease of discussion, we take "R_p" to represent the bottom profile radius. Below the table lists the relevant sources of the "R_{ini}" and "R_{fin}" under different fitting cases.

Table 4.1: The determination of R_p when fitting unloading region

	1_{st} unload	2_{nd} unload	3_{rd} unload	4_{th} unload
R_{ini}	∞	R_i	R_i	R_i
R_{fin}	R_p-1_{st} stage	R_p-2_{nd} stage	R_p-3_{rd} stage	R_p-4_{th} stage

Table 4.2: The determination of R_p when fitting unloading region

	1_{st} **reload**	2_{nd} **reload**	3_{rd} **reload**
R_{ini}	R_p-1_{st} stage	R_p-2_{nd} stage	R_p-3_{rd} stage
R_{fin}	R_i	R_i	R_i

4.2 Data processing

4.2.1 Practical fitting function

As emphasized in the analytical model establishment, equation2.28, originated from the Hertz elastic contact theory, dominates the solving procedure for effective modulus estimate. When it is applied to fit the practical output P-h data, some considerations are raised regarding the parameters defined. The practical fitting function is thus revised as:

$$P - P_f = \frac{4}{3} E_{eff} R_{eff}^{\frac{1}{2}} (h - h_f)^{\frac{3}{2}} \tag{4.2}$$

Concerning the practical data collection, the exported measured data of h involves both elastic and plastic deformation and has to eliminate the plastic contribution before processing into the fitting function. Besides, to minimize the measurement errors of the indentation load, a parameter P_f has been introduced. This was aimed at consolidating all the load measuring errors under a single parameter P_f to simplify the fitting procedure.

4.2.2 Practical fitting regions

To obtain sufficient indentation data and conduct a comprehensive analysis, four successive indentation tests are performed at one fixed point on the sample surface. There are in total 4 unloading segments and 3 reloading segments expected in the output P-h curves under the peak load case, as illustrated in the diagram 4.3. In addition, similar cyclic indentation tests are also made on other testing points but each point is subjected to a different peak load. As it is a homogeneous testing material, the indentation responses from different points can be considered representative of a single local mechanical response of the sampled material. It is thereby reasonable to compare their fitting results (of each point) under various peak loads.

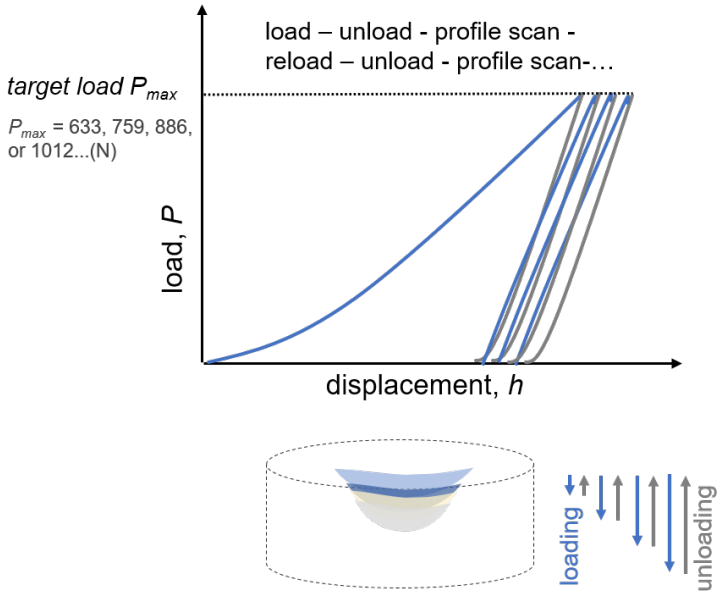

Figure 4.3: Schematic of cyclic indentation tests on one specific point

4.2.3 Determination of the effective radius

Unlike the directly measurable data of load P and depth h, it is quite complicated to acquire the effective radius R_{eff}. The main challenge lies in characterizing the curvature radius of the residual indent profile at the bottom as the deformed surface after unloading remains an unspecified shape and thus no specific mathematical model could precisely quantify the profile data.

Thus, a fifth-order polynomial fitting function was first introduced to make a rough estimate, allowing it to capture the curvature radius of every collected experimental data fairly well. The fitting region refers to the once-contact area, which is determined by the contact

area/radius estimate under the peak load using the Oliver-Pharr models. In this context, the polynomial fitting program resolves the discrete profile datasets with a credible analytical expression and can thus estimate the curvature radius distribution along the profile bottom at the same spot of the once-contact area. Relevant formulas 4.34.4 that respectively express the used high-degree polynomial fitting function and the curvature radius determination are given below. Significantly, this leads to assessing the overall shape of the residual indent surface and meanwhile is beneficial to figure out a more suitable fitting function to accurately solve the curvature radius at the bottom of the indented surface.

For the used fifth-order polynomial fitting function:

$$y = ax^5 + bx^4 + cx^3 + dx^2 + ex + f \tag{4.3}$$

Where a, b, c, d, and e are coefficients for solving.

For the mathematic formula of the radius of curvature applied in the thesis:

$$\rho = \frac{(1 + (y'(x)^2))^{\frac{3}{2}}}{|y"(x)|} \tag{4.4}$$

"$y = f(x)$" is the analytical expression of the target curvature and here it is substituted by the polynomial expression obtained from fitting.

In this thesis, an additional fitting procedure using the Least Square Circle Fit (LSCF) has been conducted for some certain indent cases, which were evaluated to possess a high level of circularity by the preliminary polynomial fitting program. As one of the widely applied circle-arc-fitting algorithms, LSCF is considered particularly useful when dealing with discrete arc-shaped datasets. Its goal is to find the best-fitting circle to a set of data points by minimizing the sum of the squared differences between the distances from the data points to the fit circle. Compared to other algorithms like nonlinear optimization, it provides a relatively accurate estimation and proves to be more computationally efficient when applied to our uncomplicated fitting task.

To sum up, a high degree (fifth) of polynomial function is primarily to make a rough assessment of the overall shape of the residual indent surface. As for some indent cases with a high circularity level, another fitting program of the Least Square Circle Fit is further employed to accurately capture their profile radii. The primary objective of combining the two fitting programs is to initially identify certain indent cases through the polynomial fitting, wherein the once-contact areas are more straightforward to characterize. Building on this foundation, the aim is to reduce R_p measurement errors associated with the spherical-like indent case by means of the LSCF and facilitate a more reliable estimate of the effective radius.

4.3 Experiment setup

Indentation experiments were carried out at room temperature using the indentation plastometer benchtop machine produced by Plastometrex Ltd, as presented below4.4. A silicon nitride (Si_3N_4) spherical indenter of 1.006 mm radius was adopted. Such size of the indenter satisfies adequate indent area that covers a great assembly of grains for a representative mechanical response[15]. Generally speaking, DH36 steel has a fine-grained microstructure and its grain size typically falls within the category of ASTM grain diameter of approximately 5.5 to 17.5 micrometers[39]. Compared to the indenter size which is almost 60 180 times larger, the indent diameter has covered sufficient grains.

and it also ensures a large penetration under a relatively smaller indentation load. Concerning the profile data extraction, a stylus profilometer with a resolution of about 1 μm was used to measure the radial distance between the indentation axis and the edge, and the corresponding height from the original sample surface. Besides, according to instructions in the user manual, each indent should not be located within 6 mm of another existing indent or 3 mm of a free edge. Hence maximum of 4 indentations were carried out on each (8 X 27 mm) testing region. (There are two same scopes of regions adjacent to each other in one D-series sample, as shown in the schematic4.5.)

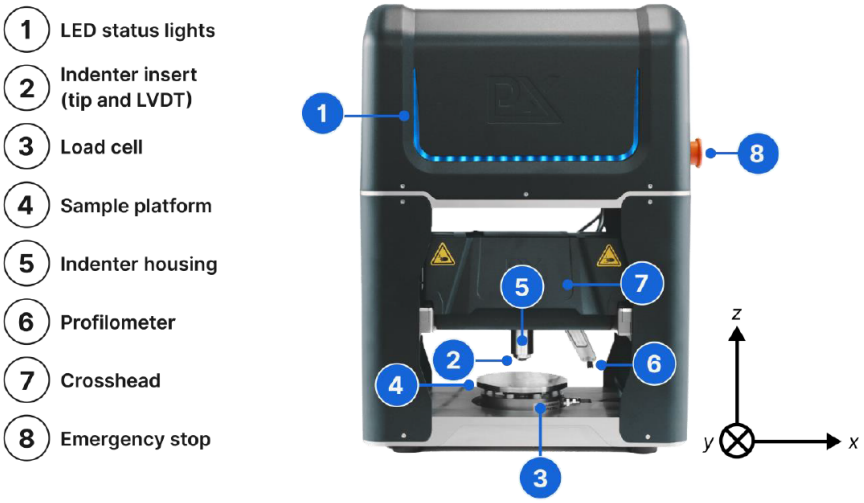

Figure 4.4: The used indentation testing instrument Plastometer and its key components[30]

4.3.1 Operation parameters setting

When running the operation program of the indentation plastometer, three main parameters were preliminary reset in obtaining the intermittent residual profile data and load-displacement curves under the advanced mode of the embedded CORSICA operation sys-

Table 4.3: Three key parameters for adjustments in advance mode of Plastometer

Control parameter	before	after	Remark
minimal indentation depth before achieving load point	110 μm	10 μm	Load-displacement data is also well addressed in the postprocess part. The modification assists in collecting more instrument data.
max_work_hardening_parameter	0.05	50.05	
Manual Load Point (the maximum target load depends on the default setting)	0 N	Set the value of the target load (N), separately, such as 506, 633, 759, 886,1012 ...	

tem. They are shown in the table4.3 below:

It should be noted that the maximum loads were set following 506, 633, 759, 886, 1012. This was to comply with the PIP working principles in terms of inferring properties, that the target manual loads must equal to the following load increments of 125 N*1.006^2 (1.006 is the indenter radius) when in the range of 125 N to 2500 N. So the load increments will follow 127N, 253N, 379N, 506, 633, 759, 886, 1012, 1265....The deformation rate during indentation was always set constant with the system default value of 400 μm/s, while it turns to 50 μm/s in the unloading mode before the indenter is not in contact with the sample surface anymore.

4.3.2 Profile take

The definite experimental procedures within the indentation plastometer are as follows: (a) Place a sample on the test platform and perform an indentation test by clicking "start" bottom. A load-displacement curve was collected automatically once the load frame was lifted. (b) go to "Tools" in the menu bar and take an individual profile of the residual indent by clicking the "Take Profile". This is due to the "shallow" indents we expected from the set peak loads. There is a certain threshold standard for the indent whether it is shallow or not from its IFEM operation system (in this case, the threshold of the applied peak load is 1012 ascertained by the output target load using normal operating mode). Thus an extra single profile taking is made if the peak load doesn't reach 1012 since such measurement can not be automatically worked after indentation.

4.3.3 Sample preparation

In this thesis, the provided steel DH36 sample was assumed to be homogeneous. We acquired Young's modulus of the steel sample through both uniaxial tensile tests and the de-

veloping indentation-based approach. In this case, the local elastic response is supposed to be equivalent to the bulk one, allowing the obtained local elastic property from the novel way to be suitable for comparison with the tensile result. Specifically, two tensile specimens were originally cut at angles of 45°, and 90° to the rolling direction of the DH36 sample. Each of their loading direction follows the same cut direction when the tensile samples perform the uniaxial tensile tests. Whereas as for the indentation-based approach, it is more convenient to investigate the anisotropic issues that simply altering the indentation plane changes the loading direction. To correspond with the tensile results, we prepared two indentation samples with surface plane directions at 45°, and 90° to the rolling direction (the surface direction aligned with its normal line), labeled as "D45" and "D90", respectively. Among them, the D90 sample was directly provided by the Georgia Institute of Technology. There are two adjacent rectangular surfaces of the same size 8 X 27 (mm) as the test region. Relevant sample information is illustrated in Figure4.5

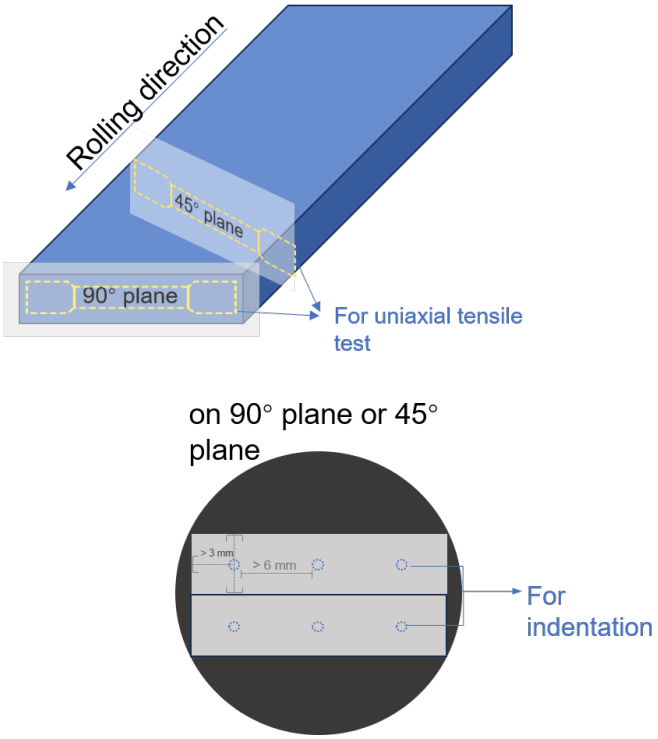

Figure 4.5: Schematic of sample preparation in uniaxial tensile tests and indentation tests

The sample D45 was cut (with a Struers Discotom-6 cutting machine) into two cuboids with the same size of 8 X 18 (mm) for the indentation plane. It was then hot-mounted using the Struers CitoPress-5 mounting equipment (185$^c icleC$ heating for 6 min, and quickly cooling for 10 min). Mechanical grinding and polishing were next conducted with both two samples on a series of Struers manual equipment to achieve a deformation-free surface as

well as possible. The specific surface technique follows the same description in Chapter "Semi-analytical model".

4.4 Results

4.4.1 Extraction of effective radius

As given from tables 4.24.1 that clarifies the constituents of effective radius under unloading or reloading case, the main challenge to extracting effective radius is to figure out the profile radius R_p, which refers to the radius of curvature at the bottom of the residual indent profile. This subsection presents the relevant results on R_p determination.

4.4.1.1 Profile fitting results through fifth-order polynomial function

Below are the profile-fitting results with the fifth polynomial function. The profile data of both D90 and D45 samples demonstrate a very high degree of goodness-of-fit, with the residuals approximate 10-4e. (Note, the fitting data is confined to the range of 0.95"a" from the original raw data, specifically focusing on the deformation area of the sample surface.)

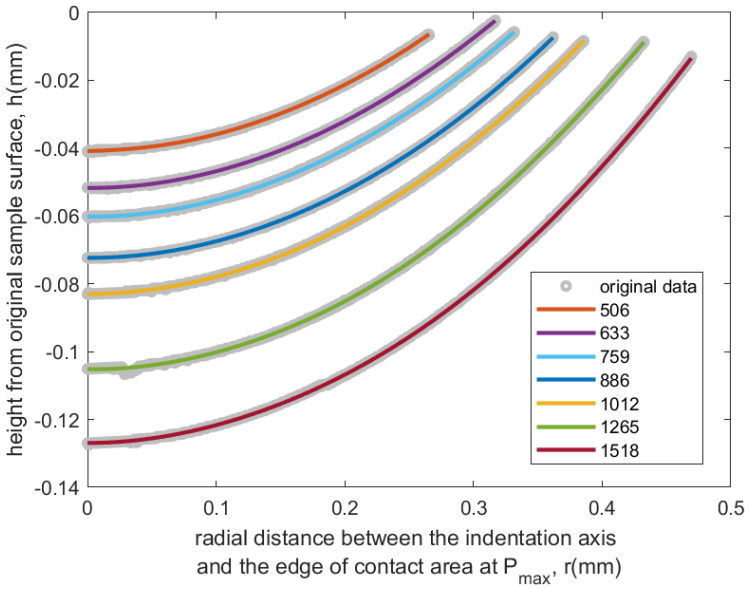

Figure 4.6: Results of 5-order polynomial fitting (D90 sample)

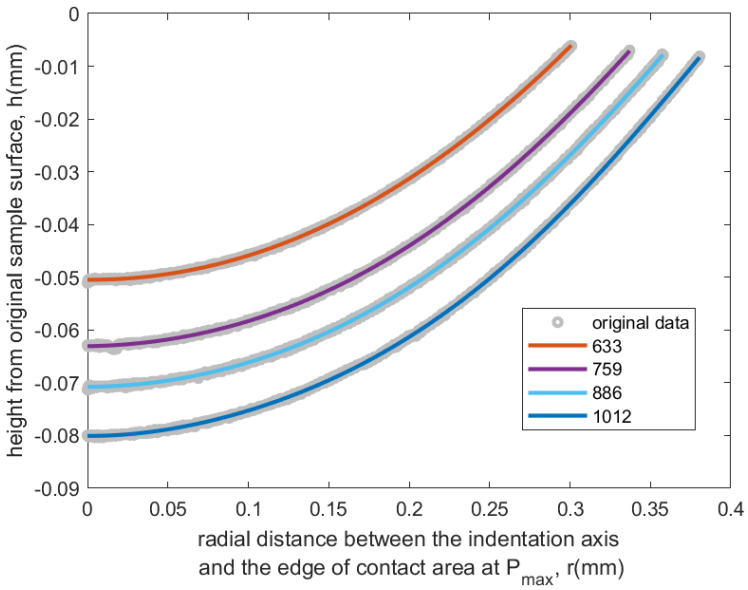

Figure 4.7: Results of 5-order polynomial fitting (D45 sample)

Utilizing the analytical fifth-order polynomial fitting method, it becomes feasible to establish the curvature radius distribution across the same cope of the datasets. Take the example of the D90 sample case. The following diagrams4.8 compare the curvature radius distributions of the profile data from a single indentation test but under different target loads.

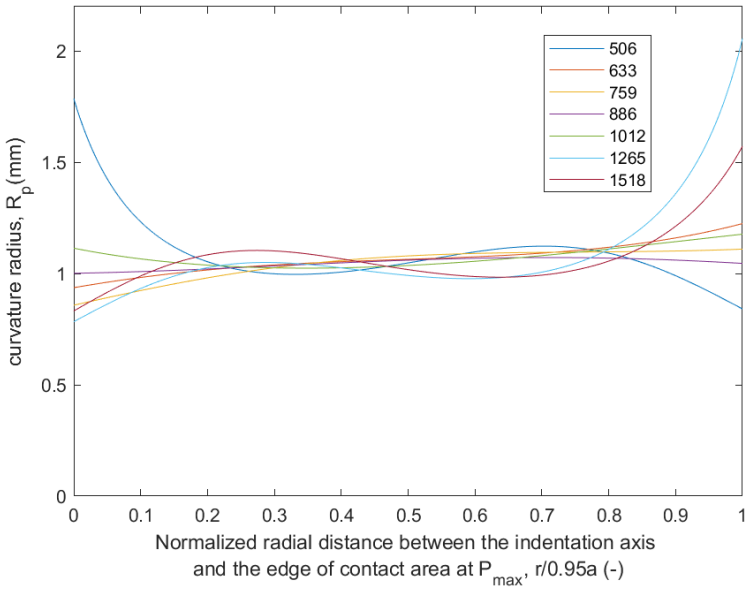

Figure 4.8: Curvature radius distributions under different target load cases (D90 sample)

From this diagram, the curvature radii under the target loads at 633, 759, 886, and 1012 are distributed uniformly, causing a relatively higher circularity level for the corresponding residual indent. It indicates a shallow indentation is much more likely to produce an indented bottom with a spherical surface. In this scenario, this allows for a more accurate determination of profile radius through the circle fit approach.

Meanwhile, a series of repeated indentation tests were also performed under those target loads and output the profile data in different stages of the cyclic indentation tests. Take the same fitting method as above, their curvature radius distributions are shown in the diagram4.9 below:

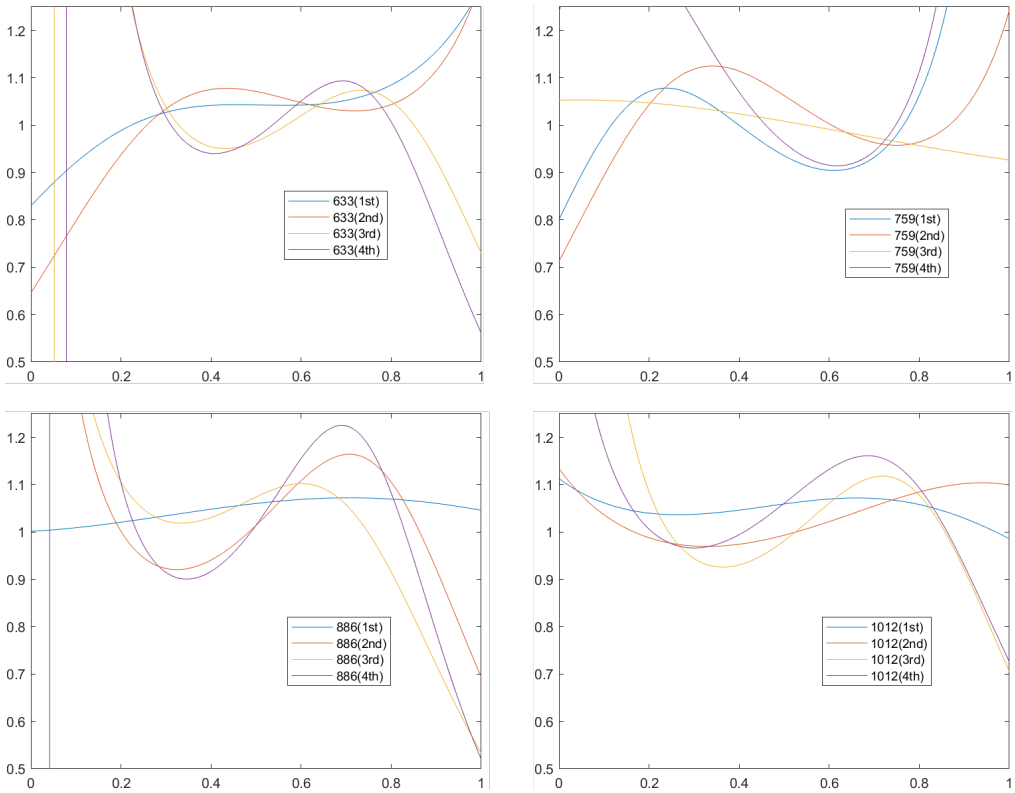

Figure 4.9: curvature radius distribution under different stages of cyclic indentation tests (D90 sample)

By comparing the curvature radius distributions from those staged profiles, the curvature radii along the once-contact area are more gently distributed with the increase of the target load. However, it is still recognized that the detected surface shows less tendency to be spherical after the repeated indentation under all the target cases.

4.4.1.2 Profile radius estimates through Least Square Circle Fit

Based on the above results, we adopt the Least Square Circle Fit (LSCF) method to further figure out the profile radius under the cases of single indentation test with the target loads at 633, 759, 886, and 1012 N. To maintain accuracy, Specially, we use both the "X" scanning data and "Y" scanning data. Relevant profile radius results are listed in the tables4.44.5 below.

Table 4.4: Profile radius outcomes by "X" scanning (D90 sample)

Target load [N]	633	759	886	1012
$R_{LSCF}[mm]$	1.0354	1.0287	1.0388	1.0370

Table 4.5: Profile radius outcomes by "Y" scanning (D90 sample)

Target load [N]	633	759	886	1012
$R_{LSCF}[mm]$	1.0367	1.0381	1.0323	1.0365

The above fitting results of profile radius through the LSCF method demonstrate an irregular pattern due to the limited amount of results. Hence, we compare each of them with the aforementioned curvature radius distribution in the corresponding case, as shown in the diagrams 4.104.11.

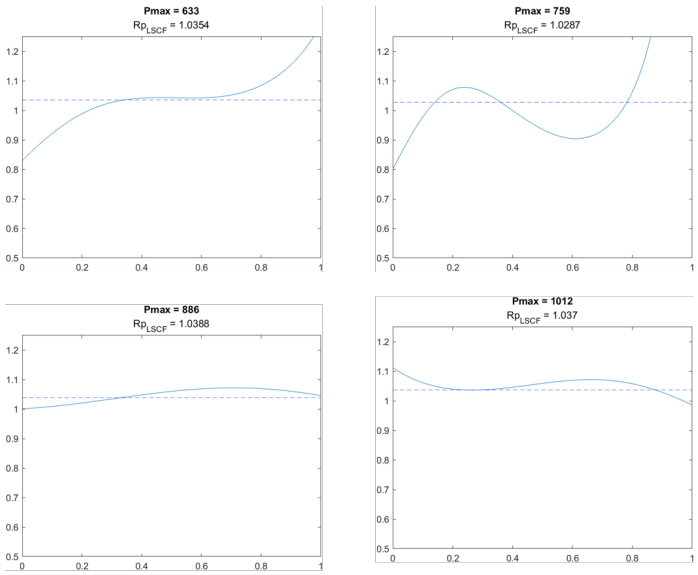

Figure 4.10: Curvature radius comparison between polynomial fitting and LSCF fitting, under "X" direction scanning (D90 sample)

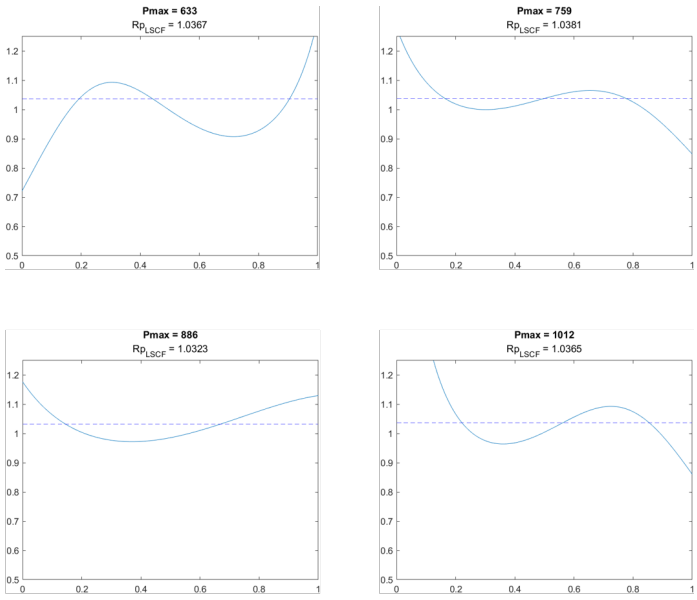

Figure 4.11: Curvature radius comparison between polynomial fitting and LSCF fitting, under ”Y” direction scanning (D90 sample)

Clearly, under various peak load scenarios, all the LSCF-fitted radii fall within the range of curvature radii distributed along the once-contact region. In particular, each fitted radius is prone to approaching the median or mean value of curvature radii estimated by the polynomial fitting. This somewhat indicates the LSCF method’s fairly high accuracy in solving the profile radius at the bottom. Nevertheless, compared to the profile data acquired through the ”X” direction, the scanning results in the ”Y” direction (perpendicular to the ”X” direction) manifest a relatively larger variation in the curvature radius distribution, which reveals a lower circularity level of the residual once-contact surface. As the operation system of the Plastometer usually takes the ”X”- scanning result as the default output of the residual indent profile, rather than the ”Y”-scanning one. it suggests some measurement error in the data acquisition of the profilometer when switching scanning directions, and scanning in the ”X” direction is supposed to provide the most accurate depiction of the actual profile. Hence, only profile data from X-direction scanning is used for further data processing.

4.4.1.3 Overview of the obtained effective radius

Based on the above results, the credible effective radius extraction is confined to the first unloading and the first reloading segments at the target loads ranging from 633 N, 759 N, 886 N, and 1012 N. This is because their corresponding profile radius can be identified with high credibility. Relevant experimental R_{eff} outcomes from D45 and D90 samples are summarized in the tables4.64.7. Note, in the result part, we mostly present the data from D90 for a clear layout. Data from D45 shows the same trend, and some of its specific information has been put in the appendix for check.

Table 4.6: Effective radius estimates under different target loads in D45 sample case

Target load [N]	Unloading			Reloading		
	Rini [mm]	Rfin [mm]	Reff [mm]	Rini [mm]	Rfin [mm]	Reff [mm]
633	1.006	1.0475	25.392	1.0475	1.006	25.392
759	1.006	1.0468	25.811	1.0468	1.006	25.811
886	1.006	1.0439	27.709	1.0439	1.006	27.709
1012	1.006	1.0381	32.534	1.0381	1.006	32.534

Table 4.7: Effective radius estimates under different target loads in D90 sample case

Target load [N]	Unloading			Reloading		
	Rini [mm]	Rfin [mm]	Reff [mm]	Rini [mm]	Rfin [mm]	Reff [mm]
633	1.006	1.0354	35.429	1.0354	1.006	35.429
759	1.006	1.0287	45.589	1.0287	1.006	45.589
886	1.006	1.0388	31.861	1.0388	1.006	31.861
1012	1.006	1.0370	33.652	1.0370	1.006	33.652

4.4.2 Fitting with the Hertz elastic equation

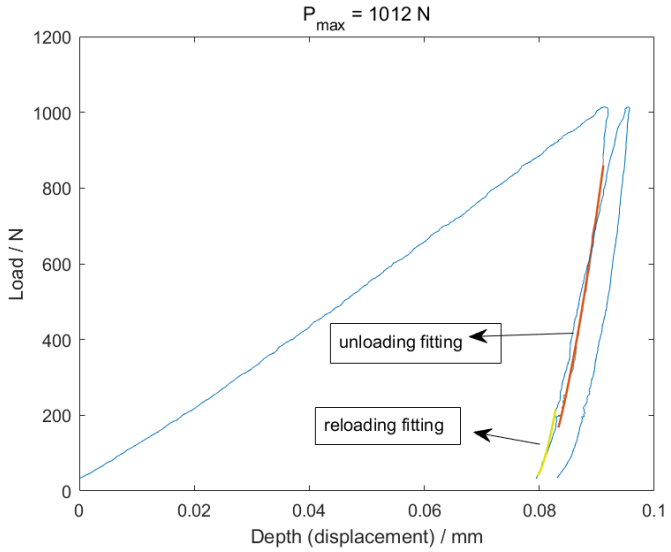

Figure 4.12: The schematic of the unloading/reloading fitting procedure. (Take the example of the target load of 1012 N)

Above is the schematic of the fitting output with the Hertz elastic equation. The unloading segment of the middle section has been fitted with the Hertz equation, resulting in the fitting represented by the orange curve. Meanwhile, the initial reloading phase has also been fitted, with the fitting results depicted by the yellow curve. The effective modulus fitting results for D45 and D90 samples, obtained from both the unloading and reloading cases, are presented in Tables 4.8 and 4.9. In general, the effective modulus estimates for the D45 sample are lower than those for the D90 sample, especially in cases with the lowest (633 N) and highest (1012 N) target loads. Furthermore, when comparing results between unloading and reloading segments, effective modulus estimates from reloading always exhibit a lower value, ranging from 48% to 80% of that obtained from the comparable unloading case under the same target load.

Table 4.8: Effective modulus estimates under different target loads (D45 sample)

Target load [N]	E_{eff} / GPa in unloading case	E_{eff} / GPa in reloading case
633	68	54
759	128	61
886	104	56
1012	92	62

Table 4.9: Effective modulus estimates under different target loads (D90 sample)

Target load [N]	E_{eff} / GPa in unloading case	E_{eff} / GPa in reloading case
633	122	90
759	145	75
886	134	97
1012	118	76

4.5 Discussion

4.5.1 Discrepancy between D45 and D90 samples

According to the effective radius results, both the unloading and the subsequent reloading scenarios are analyzed to be able to fit with the Hertz contact model. Specifically, the bottom profile after a single indentation exhibits a spherical-like shape under target loads ranging from 633 N to 1012 N. A more accurate circle fitting method is then employed to extract the profile radius with high credibility and provide reliable determinations of the effective radius.

Based on the provided tensile results from the two analogous samples, with a tensile modulus of 210 GPa for the comparable D45 sample and 204 GPa for the comparable D90 sample, the DH36 steel sample exhibits no obvious elastic-anisotropic feature. It is thus expected that there would be no significant difference in the effective modulus estimates between the D90 sample and D45 sample under the same indentation testing system. However, the practical results fail to meet this expectation. For the D90 sample, its effective modulus estimates show relatively minor differences between 118-146 GPa, with a small standard deviation of 12.2 in the unloading case and 10.8 in the reloading case. In contrast, the obtained effective modulus for the D45 sample falls within a wide range of 68-128 GPa, exhibiting a greater standard deviation of 25.0 in the unloading case and a smaller standard deviation of 3.9 in the reloading case. It suggests a lower measurement precision for the D45 sample.

The main difference between the two samples, aside from the cutting direction aspect, lies in their respective mounting materials. Compared to the sturdy mounting material utilized for the provided D90 sample, the mounting material used for the D45 sample appears to be less rigid and stable. This might provide insufficient stability and rigidity to support the steel material during indentation tests. Therefore, the measured displacement may also count the undesired deformations or compression from the mounting material beneath the testing steel, potentially leading to inaccurate measurements of the sample's mechanical properties.

4.5.2 Discrepancy between unloading and reloading cases

The unload and initial reload processes exhibit a similar P-h curve trend from Figure**??**, suggesting the changes in displacement are almost reversible with the applied load. This to some extent explains why the unloading and the following beginning part of reloading could be treated as elastic segments. In a real-world context, the two scenarios respectively reflect the state where the sample is pressed by the indenter and the state where the indenter is pressed by the sample. Theoretically, the two should be consistent since the forces involved are reciprocal.

However, in practical measurements, the two segments could not be perfectly overlapped. In principle, this can be explained that the sample inevitably experiences some levels of inelastic strains during the initial contact with the indenter in the reloading procedure. As for the errors caused by practical measurement, the predominant experiment errors are more likely attributed to the data-collecting system of the instrument used. The load cell, located at the bottom (see its position in Figure 4.4), measures the downward force and may work differently when the indenter system applies force to the sample surface, compared to when the sample surface applies the same force to the upper indenter systems. Investigating such discrepancy displayed in the P-h curves, to some extent, may reveal the load compliance information about the testing system.

Chapter 5

Conclusions and recommendations

5.1 Conclusions

In this thesis, a semi-analytical model, which aims to extract a material's Young's modulus and yield strength, was validated using our own hardware testing system. Meanwhile, based on the elastic unloading and reloading responses of the testing material, an analytical model was developed to acquire the material's elastic modulus. Both models are established with the same purpose to convert indentation data for a material's mechanical properties.

5.1.1 A semi-analytical model validation

In the first research topic with the semi-analytical model, an overview of the resulting estimates, both from example data and in-house data, is given in the table below, along with the uniaxial tensile test reference values.

Table 5.1: Results overview in validating the semi-analytical model

	Exampledata	In-house data	Tensile results
Young's modulus estimate	209 GPa	37 GPa	204±7 GPa
Yield strength estimate	387 MPa(Hertz model) 392 MPa(Oliver-Pharr model) 420 MPa(Relative Stiffness model)	Fail for all contact radius models	391±0 MPa
Hardware Remark	• Zwick/Roell Z100 • 6.35 mm indenter • Testing sample DH36 steel • 15 load-unload cycle • P_{max} of around 150 N	• ZwickRoell Z2.5 • 14.00 mm indenter • Testing sample DH36 stee • 15 load-unload cycle • P_{max} of around 100N	-

It was found that the semi-analytical model failed to capture the yield point, and there was a significant error in Young's modulus estimates using the experimental data from the in-house hardware testing system, with more than an 80 % error to the tensile reference value. However, this model works well with the example data with a comparable testing

system. Preliminary analysis suggests that the current test system does not capture data related to the initial contact procedure. This might be owing to sensing issues regarding load or displacement, leading to an invalid surface detect. Thus it can be concluded that the model is incompatible with our own testing system.

5.1.2 A novel analytical model for effective modulus extraction

In addressing the practical problems met by the semi-analytical model mentioned above, we have developed an analytical model that extracts a material's Young's modulus through the unloading responses, with the extra help of profilometry. For the analytical model, its establishment involves a key part of characterizing the profile radius. Here are some key conclusions drawn from the result analysis:

1. The 5th-order polynomial fits the profile data well, but there exhibits a large error when attempting to obtain a representative profile radius by calculating the curvature radius at each point of the fitted curve.

2. Nevertheless, the curvature radius distribution derived from the 5th-order polynomial fitting can be used to assess the circularity level of the profile bottom. Shallow indentation cases, with target loads ranging from 633, 759, 886, and 1012N possess high circularity levels.

3. For cases with high circularity levels, the profile radius can be more accurately evaluated using the least square circle fit method.

Furthermore, regarding the model testing concerning different fitting regions and sampled materials, below list some key conclusions drawn from the result analysis:

1. The effective modulus estimates from the first unloading segment in both sample cases are the closest to the tensile reference value, with an average deviation error of 6 %. While it reaches 41% for the reloading case.

2. The effective modulus estimates from the D90 sample are more reliable compared to those from the D45 sample. The estimates from D90 closely align with the reference values from uniaxial tensile tests, with an error of less than 20%. While the error even reaches 44% for the latter D45 sample case.

5.2 Recommendations

The validation of the semi-analytical model highlights its strong reliance on the initial datasets that cover a material's pure elastic responses, yet this can not be achieved by our in-house testing system. **Further recommendations can not only refer to the adjustments in instrument calibration but also to optimize or develop an alternative effective**

modulus model that is less reliant on the initial indentation data capturing.

As for the developed analytical model, there exhibits significant result discrepancy between D45 and D90 samples, while their analogous tensile modulus did not show very strong anisotropic features. Probably reason can be attributed to the different mounting materials they use. **Further work is needed to clarify this influencing factor and establish specific criteria for the mounting material used for sampling.** Other recommendations about model practicality are summarized below:

1. Enhance the resolution of the profilometry particularly at the bottom of the residual indent profile.

2. Optimize the algorithm for extracting the curvature radius at the profile bottom.

3. Establish specific criteria for the mounting material used for sampling, at least providing sufficient stability and rigidity to support the testing material.

Bibliography

[1] WM Thomas et al. *International patent application no*. Tech. rep. PCT/GB92/02203 and GB patent application, 1991.

[2] *What is friction stir welding of aluminum?* 2013. URL: http://www.esabna.com/us/en/education/knowledge/qa/What-is-friction-stir-welding-of-aluminum.cfm.

[3] R. S. Mishra and Z. Y. Ma. *Friction stir welding and processing*. Aug. 2005. DOI: 10.1016/j.mser.2005.07.001.

[4] Seung-Joon Lee, Yufeng Sun, and Hidetoshi Fujii. "Stacking-fault energy, mechanical twinning and strain hardening of Fe-18Mn-0.6 C-(0, 1.5) Al twinning-induced plasticity steels during friction stir welding". In: *Acta Materialia* 148 (2018), pp. 235–248.

[5] Seung-Joon Lee, Kohsaku Ushioda, and Hidetoshi Fujii. "Evaluation of stacking-fault energy in Fe-Mn based twinning-induced plasticity steels after friction stir welding". In: *Materials Characterization* 147 (2019), pp. 379–383.

[6] Seung-Joon Lee et al. "Microstructure, mechanical properties, and damping capacity in stir zone after friction stir welding of Fe–17Mn damping alloy". In: *Journal of Alloys and Compounds* 803 (2019), pp. 1155–1167.

[7] D. Ambrosio et al. "Relationships between welding parameters, aging conditions, and weld properties in AA7075-T6 friction stir welds". In: *International Journal of Advanced Manufacturing Technology* 111.5-6 (Nov. 2020), pp. 1333–1350. ISSN: 14333015. DOI: 10.1007/s00170-020-06184-y.

[8] Pradeep Johnson and N Murugan. "Microstructure and mechanical properties of friction stir welded AISI321 stainless steel". In: *Journal of Materials Research and Technology* 9.3 (2020), pp. 3967–3976.

[9] Tom Southern et al. "Indentation Plastometry for Study of Anisotropy and Inhomogeneity in Maraging Steel Produced by Laser Powder Bed Fusion". In: *Steel Research International* 94.7 (July 2023). ISSN: 1869344X. DOI: 10.1002/srin.202200881.

[10] Gefei Liu and Gefei Liu. *Wooden barrel theory*. Apr. 2014. URL: https://www.pvisoftware.com/blog/wooden-barrel-theory/.

[11] Laura Moody. “The Effect of Thickness and Plastic Behavior on the Validity of Sub-Scale Tensile Testing of Titanium”. PhD thesis. 2021.

[12] URL: https://www.struers.com/en/Knowledge/Hardness-testing#.

[13] J. E. Campbell et al. “Comparison between stress-strain plots obtained from indentation plastometry, based on residual indent profiles, and from uniaxial testing”. In: *Acta Materialia* 168 (Apr. 2019), pp. 87–99. ISSN: 13596454. DOI: 10.1016/j.actamat.2019.02.006.

[14] J. E. Campbell et al. “Experimental and computational issues for automated extraction of plasticity parameters from spherical indentation”. In: *Mechanics of Materials* 124 (Sept. 2018), pp. 118–131. ISSN: 01676636. DOI: 10.1016/j.mechmat.2018.06.004.

[15] J. Dean and T. W. Clyne. “Extraction of plasticity parameters from a single test using a spherical indenter and FEM modelling”. In: *Mechanics of Materials* 105 (Feb. 2017), pp. 112–122. ISSN: 01676636. DOI: 10.1016/j.mechmat.2016.11.014.

[16] Laurence W. McKeen. “1 - Introduction to Fatigue of Plastics and Elastomers”. In: *Fatigue and Tribological Properties of Plastics and Elastomers (Third Edition)*. Ed. by Laurence W. McKeen. Third Edition. William Andrew Publishing, 2016, pp. 1–26. ISBN: 978-0-323-44201-5. DOI: https://doi.org/10.1016/B978-0-323-44201-5.00001-0. URL: https://www.sciencedirect.com/science/article/pii/B9780323442015000010.

[17] Sept. 2023. URL: https://en.wikipedia.org/wiki/Transfer_learning.

[18] Trevor William Clyne et al. *Profilometry-Based Inverse Finite Element Method Indentation Plastometry*. Sept. 2021. DOI: 10.1002/adem.202100437.

[19] J. Hay. “Introduction to instrumented indentation testing”. In: *Experimental Techniques* 33.6 (2009), pp. 66–72. ISSN: 07328818. DOI: 10.1111/j.1747-1567.2009.00541.x.

[20] KL Johnson. “Introduction to Contact Mechanics: a summary of the principal formulae”. In: *Fundamentals of friction: Macroscopic and microscopic processes* (1992), pp. 589–603.

[21] NA Stilwell and D Tabor. “Elastic recovery of conical indentations”. In: *Proceedings of the Physical Society* 78.2 (1961), p. 169.

[22] Ian M Hutchings. “The contributions of David Tabor to the science of indentation hardness”. In: *Journal of Materials Research* 24.3 (2009), pp. 581–589.

[23] W.C. Oliver and G.M. Pharr. “An improved technique for determining hardness and elastic modulus using load and displacement sensing indentation experiments”. In: *Journal of Materials Research* 7.6 (June 1992), pp. 1564–1583. ISSN: 0884-2914. DOI: 10.1557/jmr.1992.1564.

[24] E Meyer and Z Ver. “Contribution to the knowledge of hardness and hardness testing”. In: *Z. Ver. Dtsch. Ing* 52 (1908), pp. 645–654.

[25] David Tabor. *The hardness of metals*. Oxford university press, 2000.

[26] S Mohan et al. "Critical Evaluation of Spherical Indentation Stress-Strain Protocols for the Estimation of the Yield Strengths of Steels". In: (). DOI: 10.1007/s11340-021-00689-7/Published. URL: https://doi.org/10.1007/s11340-021-00689-7.

[27] Christian Ullner et al. "Effect and measurement of the machine compliance in the macro range of instrumented indentation test". In: *Measurement* 43.2 (2010), pp. 216–222.

[28] J Dean, JM Wheeler, and TW Clyne. "Use of quasi-static nanoindentation data to obtain stress–strain characteristics for metallic materials". In: *Acta Materialia* 58.10 (2010), pp. 3613–3623.

[29] H Pelletier. "Predictive model to estimate the stress–strain curves of bulk metals using nanoindentation". In: *Tribology International* 39.7 (2006), pp. 593–606.

[30] URL: https://plastometrex.com/blogs/a-brief-overview-of-pip.

[31] T. W. Clyne and J. E. Campbell. *Testing of the Plastic Deformation of Metals*. Cambridge University Press, May 2021. ISBN: 9781108943369. DOI: 10.1017/9781108943369. URL: https://www.cambridge.org/core/product/identifier/9781108943369/type/book.

[32] Zhihan Zhang et al. "Microstructure and anisotropic mechanical behavior of friction stir welded AA2024 alloy sheets". In: *Materials Characterization* 107 (July 2015), pp. 112–118. ISSN: 10445803. DOI: 10.1016/j.matchar.2015.06.039.

[33] Yu Su et al. "Effect of FSW process on anisotropic of titanium alloy T-joint". In: *Materials and Manufacturing Processes* 37.1 (Jan. 2022), pp. 25–33. ISSN: 1042-6914. DOI: 10.1080/10426914.2021.1942911. URL: https://www.tandfonline.com/doi/full/10.1080/10426914.2021.1942911.

[34] Harish Suthar, Anirban Bhattacharya, and Surajit Kumar Paul. "Characterizing the anisotropic response of similar and dissimilar FSW joints by DIC-based simultaneous strain measurements on two orthogonal surfaces". In: *Journal of Manufacturing Processes* 84 (Dec. 2022), pp. 697–712. ISSN: 15266125. DOI: 10.1016/j.jmapro.2022.10.036. URL: https://linkinghub.elsevier.com/retrieve/pii/S1526612522007241.

[35] Yeong Seok Lim, Sang Hyuk Kim, and Kwang Jin Lee. "Effect of Residual Stress on the Mechanical Properties of FSW Joints with SUS409L". In: *Advances in Materials Science and Engineering* 2018 (2018). ISSN: 16878442. DOI: 10.1155/2018/9890234.

[36] Kenneth Langstreth Johnson and Kenneth Langstreth Johnson. *Contact mechanics*. Cambridge university press, 1987.

[37] Surya R. Kalidindi and Siddhartha Pathak. "Determination of the effective zero-point and the extraction of spherical nanoindentation stress–strain curves". In: *Acta Materialia* 56.14 (Aug. 2008), pp. 3523–3532. ISSN: 1359-6454. DOI: 10.1016/J.ACTAMAT.2008.03.036.

[38] URL: https://www.zwickroell.com/products/hardness-testing-machines/.

[39] Arlan O Benscoter and Bruce L Bramfitt. “Metallography and microstructures of low-carbon and coated steels”. In: *Metallogr. Microstruct* 9 (2004), pp. 588–607.

Appendix A

Nomenclature

In this appendix, an overview of frequently used abbreviations and terms are given, respectively.

Abbreviations

Abbreviation	Definition
FSW	Friction Stir Weld(ing)
SZ/NG	Stir Zone or Nugget Zone
TMAZ	Thermomechanically-Affected Zone
HAZ	Heat-Affected Zone
BM	Base Material Zone
RS	Retreating Side
AS	Advancing Side
TD	Transverse Direction
ND	Normal Direction
A1	Eutectoid Temperature
FEM	Finite Element Method
IFEM	Inverse Finite Element Modeling
FDM	Finite Difference Method
IIT	Instrumented Indentation Technique
ISS	Indentation Strain/Stress
PIP	Profilometry-based Indentation Plastometry
UTS	Ultimate Tensile Strength

Symbols

Symbol	Definition	Unit
f	Friction resistance per unit length of dislocation	[N/m]
K	Work hardening coefficient or the hardening rate	[-]
n	Work hardening exponent	[-]
P	Contact force or the applied load during indentation	[N]
P^*	Load at zero point (analysis value for zero correction in actual measurement)	[N]
h	Penetration depth	[m]
h^*	Displacement at zero point (analysis value for zero correction in actual measurement)	[m]
h_t	Total penetration depth	[m]
h_c	Contact depth	[m]
h_e	Elastic depth	[m]
E	Young's modulus	[Pa]
H	Hardness value	[Pa/m^2]
E_r, E_{eff} or E_{ind}	Reduced modulus, Effective modulus or Indentation modulus	[Pa]
Y_{ind}	Indentation yield strength	[Pa]
R_i	Indenter radius	[m]
R_s	Sample radius	[m]
R_{eff}	Effective radius	[m]
A	Contact area	[m^2]
a	Contact radius	[m]
S	Elastic contact stiffness	[N/m]
S_{av}	Misfit parameters for simulations with unit	[m^2]
S_{red}	Misfit parameters for simulations in dimensionless	[-]
τ_c	Critical shear stress	[Pa]
υ	Poisson ratio	[-]
σ	Von Mises stress	[Pa]
σ_y	Yield strength	[Pa]
σ_s	Stress at a saturation level in Voce equation	[Pa]
ε	Von Mises strain	[-]
ε_0	Von Mises strain	[-]
σ_{ind}	Indentation stress	[Pa]
ε_{ind}	Indentation strain	[-]
δ	The height difference between the sample surface and the deepest point of the indent during indentation modeling in IFEM	[m]
δ/r	Penetration ratio in IFEM	[-]

Appendix B

Supplementary experimental data

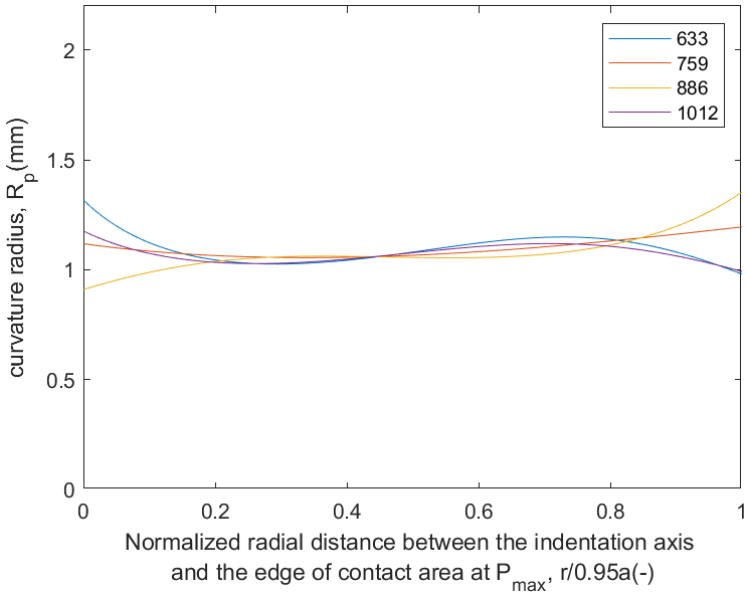

Figure B.1: Curvature radius distributions under different target load cases (D45 sample)

Table B.1: Profile radius outcomes by ”X” scanning (D45 sample)

Target load [N]	633	759	886	1012
$R_{LSCF}[mm]$	1.0475	1.0468	1.0439	1.0381

Table B.2: Profile radius outcomes by ”Y” scanning (D45 sample)

Target load [N]	633	759	886	1012
$R_{LSCF}[mm]$	1.0387	1.0433	1.0448	1.0421

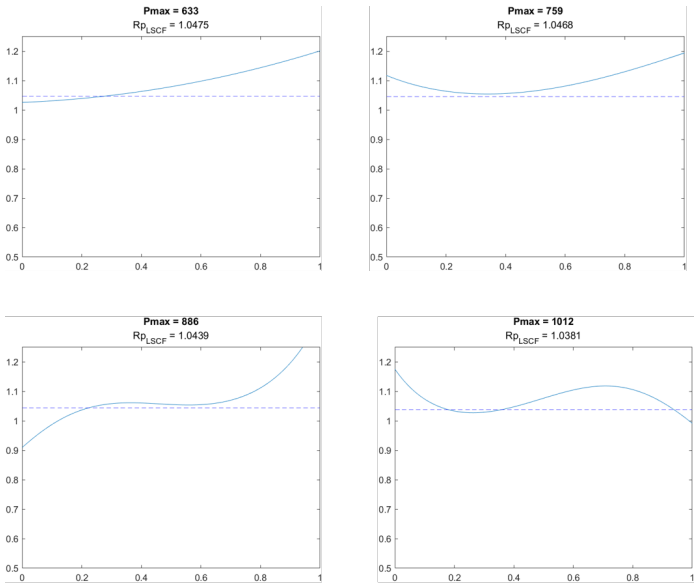

Figure B.2: Curvature radius comparison between polynomial fitting and LSCF fitting, under "X" direction scanning (D45 sample). The horizontal coordinate indicates the normalized radial distance (r/0.95a) between the indentation axis and the edge of the contact area at the peak load, while the vertical coordinate represents the corresponding curvature radius or the profile radius estimates. Same thing with the chart below.

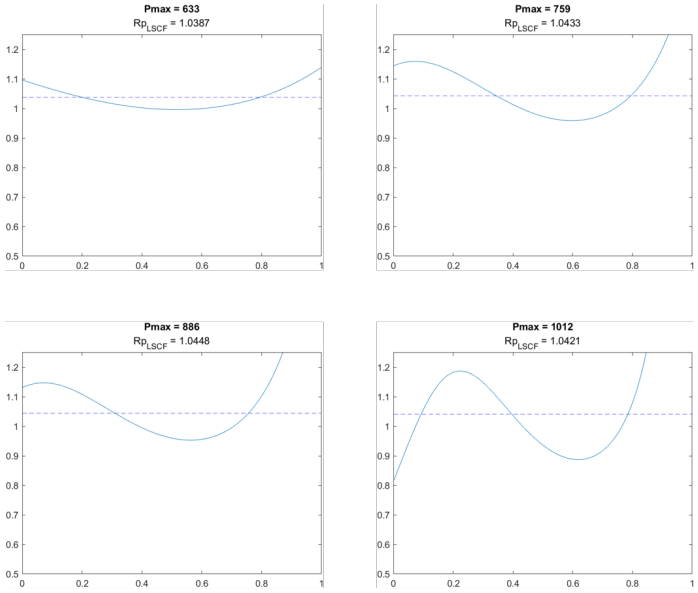

Figure B.3: Curvature radius comparison between polynomial fitting and LSCF fitting, under ”Y” direction scanning (D45 sample)